

Real-size structural health monitoring of a prestressed concrete bridge based on long-gauge fiber Bragg grating sensors

Dissertation for the Degree of Doctor of Engineering
approved by the Faculty of Civil and Environmental
Engineering at the University of Stuttgart

presented by
Felipe Isamu Harger Sakiyama
from Viçosa, Brazil

Examiner: Prof. Harald Garrecht
Co-examiner: Prof. Gustavo de Souza Veríssimo
Co-examiner: Prof. Steffen Marx

Day of the examination: 03.08.2021

Materials Testing Institute University of Stuttgart

2021

Realmaßstäbliche Überwachung einer Spannbetonbrücke (Structural Health Monitoring) auf Basis von langen Faser-Bragg-Gitter-Sensoren

Von der Fakultät Bau- und Umweltingenieurwissenschaften der Universität
Stuttgart zur Erlangung der Würde eines Doktor-Ingenieurs (Dr.-Ing.)
genehmigte Abhandlung

Vorgelegt von
Felipe Isamu Harger Sakiyama
aus Viçosa, Brasilien

Hauptberichter: Prof. Harald Garrecht
Mitberichter: Prof. Gustavo de Souza Veríssimo
Mitberichter: Prof. Steffen Marx

Tag der mündlichen Prüfung: 03.08.2021

Materialprüfungsanstalt Universität Stuttgart

2021

*To my beloved son
Pedro Zen*

Summary

The ability to track the structural condition of existing structures is one of engineers, governments, and estate managers' main concerns. In bridge maintenance programs, for example, visual inspection predominates nowadays as the primary source of information. Nonetheless, visual inspections alone are insufficient to satisfy the current needs for structural safety assessment. The increasing demand for civil infrastructures, the aging of existing assets, and the strengthening of safety and liability laws have led to the inclusion of structural health monitoring (SHM) techniques into the structural management process. With the latest developments in the sensors field and computational power, real-scale SHM deployment has become logistically and economically feasible. However, it is still challenging to perform a quantitative evaluation of the structural condition based on measured data. Although the current approaches of SHM systems using traditional single-point sensors – such as electric strain sensors, accelerometers, and GPS-based sensors – have appropriate measurement precision for SHM purposes, they present challenges when deployed in real-scale applications, given the limited number of possible points to assess the structural behavior and the harsh environmental conditions during operation. When it comes to prestressed and reinforced concrete structures, structural monitoring and damage identification present further challenges. They are affected by various chemical, physical and mechanical degradation processes and have a heterogeneous composition and non-linear behavior. On the other hand, fiber optic (FO) technology can provide integrated sensing in extensive measurement lengths with high sensitivity, durability, and stability, making them ideal for SHM of concrete structures. From this perspective, extensive research on structural health monitoring has been developed in the last decades. However, the transfer rate from laboratory experiments to real-case applications is still unsatisfactory. This research addressed the main limitations that slow the deployment and the acceptance of real-size structural health monitoring systems in

bridge maintenance programs. It proposed a long-term SHM concept to monitor prestressed concrete bridges, enabling the real-time detection of inherent damaging processes such as prestressing tendon break and crack opening and providing meaningful structural information to support decision-making within bridge maintenance programs. An SHM system based on long-gauge fiber Bragg grating (LGFBF) sensors was designed and deployed in a real-size prestressed concrete bridge. Autonomous and intelligent measurement tasks with data management and post-processing tools were implemented to operate the SHM system and delivery the expected results. A novel runtime algorithm for real-time analysis based on random variables correlation for condition monitoring was implemented to automatically detect unexpected events, such as local structural failure, within many random dynamic loads. Additionally, an integrated methodology for data interpretation and model updating built on data feature extraction using the principal component analysis (PCA), finite element (FE) modeling, and Monte Carlo simulations was proposed to identify existing damages and optimize the FE model updating process. The results showed that the deployed SHM system successfully translates the massive raw data into meaningful information to access structural response, predict damage formation, and calibrate a FE model of the monitored structure. Finally, the proposed real-time analysis algorithm delivers a reliable notification system that allows bridge managers to track unexpected events as a basis for decision-making.

Zusammenfassung

Die Instandhaltung bestehender Ingenieurbauwerke ist eines der wichtigsten Hauptanliegen von Ingenieuren, Regierungen und Immobilienverwaltern. Bei Brückenprüfungsverfahren dominiert heutzutage zum Beispiel die visuelle Inspektion als primäre Informationsquelle. Dennoch reichen visuelle Inspektionen allein nicht aus, um die aktuellen Anforderungen an sicherheitsrelevanten Bewertungen zu erfüllen. Aufgrund der steigenden Nachfrage nach Infrastrukturen, der Alterungsprozessen bestehender Bauwerke und der Verschärfung von Sicherheits- und Haftungsgesetzen ist die Überwachung des Zustands von Strukturen (SHM) in das Qualitätsmanagementsystem aufgenommen worden. Mit den neuesten Sensor- und Computerentwicklungen wurde der Einsatz von realmaßstäblichen SHM logistisch und wirtschaftlich möglich. Es bleibt jedoch die Herausforderung, die quantitative Bewertung des Bauwerkszustands auf Basis gemessener Daten durchzuführen. Obwohl die traditionellen Einzelpunktsensoren, wie zum Beispiel elektrische Dehnungssensoren, Beschleunigungssensoren und GPS-basierte Sensoren, eine geeignete Messgenauigkeit für SHM-Zwecke aufweisen, stellen sie Herausforderungen für die Anwendung auf Brückenbauwerken dar, aufgrund der begrenzten Anzahl möglicher Messpunkte und der rauen Umgebungsbedingungen. Spann- und Stahlbetonkonstruktionen stellen weitere Herausforderungen bei der Bauwerksüberwachung und Schadenserkenkung dar. Sie sind von verschiedenen chemischen, physikalischen und mechanischen Abbauprozessen betroffen und weisen ein heterogenes und nichtlineares Verhalten auf. Andererseits bietet die faseroptische (FO) Technologie integrierte Sensorik über große Messlängen mit hoher Genauigkeit, Haltbarkeit und Stabilität, was ideal für SHM im Rahmen von Betonstrukturen ist. Aus diesem Blickwinkel heraus wurden in den letzten Jahrzehnten umfangreiche

Forschungsarbeiten zur Bauwerksüberwachung durchgeführt. Allerdings ist die Übertragungsrates von Laborexperimenten auf Industrieanwendungen immer noch nicht zufriedenstellend. Diese Dissertation befasste sich mit den wichtigsten Einschränkungen, die den Einsatz und die Akzeptanz von SHM-Systemen in Brückeninstandhaltungsprogrammen verlangsamen. Es wurde ein Langzeit-SHM-Konzept zur Überwachung von Spannbetonbrücken vorgeschlagen, um die Echtzeiterkennung von Schädigungsprozessen, wie Spanngliedbruch und Rissbildung, zu ermöglichen und aussagekräftige Strukturinformationen zur Unterstützung der Entscheidungsfindung innerhalb von Brückeninstandhaltungsprogrammen zu erzeugen. Es wurde ein SHM-System auf Basis von LGFBF-Sensoren (Long-Gauge Faser-Bragg-Gitter) entworfen und an einer Spannbetonbrücke eingesetzt. Autonome und intelligente Messungen verbunden mit Datenmanagement- und Auswertungswerkzeugen wurden implementiert, um das SHM-System zu betreiben und die erwarteten Ergebnisse zu liefern. Ein neuartiger Laufzeitalgorithmus für die Echtzeitanalyse, basierend auf der Korrelation von Zufallsvariablen für die Zustandsüberwachung, wurde implementiert, um automatisch unerwartete Ereignisse, wie zum Beispiel lokales strukturelles Versagen, innerhalb zufällig dynamischer Belastungen zu erkennen. Zusätzlich wurde eine integrierte Methodik zur Dateninterpretation und Modellaktualisierung entwickelt, die auf der Faktorenextraktion mit Hilfe der Hauptkomponentenanalyse (PCA), der Finite-Elemente-Modellierung (FE) und Monte-Carlo-Simulationen basiert, um vorhandene Schäden zu identifizieren und den FE-Modellaktualisierungsprozess zu optimieren. Die Ergebnisse zeigten, dass das eingesetzte SHM-System die große Anzahl von Rohdaten erfolgreich in aussagekräftige Informationen übersetzt, um auf das Bauwerksverhalten zuzugreifen, die Schadensbildung vorherzusagen und das FE-Modell der überwachten Struktur zu kalibrieren. Schließlich liefert der implementierte

Echtzeit-Analysealgorithmus ein zuverlässiges Benachrichtigungssystem, das es Brückenmanagern ermöglicht, unerwartete Ereignisse zu überwachen und als Grundlage für die Entscheidungsfindung zu nutzen.

This research work was collectively funded by the research agency CAPES – Brazilian Federal Agency for Support and Evaluation of Graduate Education (grant no. 001) – and the Regierungspräsidium Stuttgart (RPS, Germany).

Contents

Summary	i
Zusammenfassung	iii
1. Introduction	1
1.1. Motivation	1
1.2. Structural health monitoring of real-size concrete structures.....	4
2. Aim and objectives.....	8
3. B27 Bridge in Neckarsulm.....	10
4. Deployment of a fiber-optic-based SHM system	13
4.1. Quasi-distributed fiber-optic sensors	14
4.2. Long-gauge FBG sensors	17
4.3. The SHM system design	19
4.4. Data management system	25
5. A novel runtime algorithm for the real-time detection of unexpected structural changes.....	27
6. Damage identification and FE model updating.....	31
6.1. PCA method	32
6.2. Identifying and classifying heavy vehicles' crossing.....	34
7. Implemented scripts.....	43
8. List of publication	57
References.....	59

1. Introduction

1.1. Motivation

Transportation infrastructures are high-cost assets that play a vital role in socio-economic activities (Frischmann 2012). Particularly large structures such as highway bridges provide means to connect people, improve traffic flow at complex crossroads, shorten travel time, and provide access to places otherwise inaccessible. In this sense, the costs of an inoperant bridge, as well as the life-threatening consequences of a damaged and unattended bridge network, can be incalculable. Even so, a considerable number of these structures are reaching the end of their intended design lives (An, Spencer & Ou 2015) or have surpassed safety and serviceability limits due to changes in the design assumptions such as increasing traffic loads, the minimal amount of shear reinforcement and temperature loads, and due to material related damaging process such as fatigue aging, stress corrosion cracking of prestressed steel, and interior rotting of timber elements (Lünser 1999; Rommerskirchen et al. 2007; Aicher, Leitschuh & Hezel 2015).

For example, about 70% of the German's bridge network are prestressed concrete structures (Ahrens & Sanio 2014), and more than 50% of its highway bridges were erected until the '70s (Figure 1). At that time, design assumptions and construction materials that today are known to be erroneous and inappropriate were broadly employed. To name a few, it was not until the 80's that temperature variation was included as a load case in design codes, and the use of prestressing steels subjected to stress-corrosion-cracking was at its high peak in the '60s and '70s (Fischer et al. 2016).

In Brazil, a recent study has shown that almost 50% of the country's highway bridges are problematic (Figure 2), with 5% critically damaged (ASCOM/DNIT 2015). Moreover, the increasing demand for transportation infrastructure has raised commercial vehicles' traffic volume and load capacity (CNT, SEST & SENAT 2015; CNT 2015). While the latest design standard specifies a minimum trainload of 450 kN for highway bridges (ABNT 2013), more than 90% of Brazil's were designed with trainloads ranging from 240 kN to 360 kN (Mendes 2009).

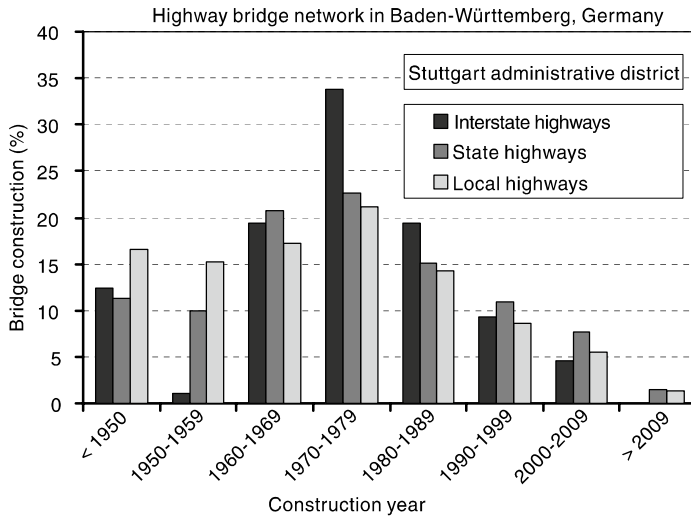


Figure 1. Construction year of highway bridges in the state of Baden-Württemberg, Germany. Adapted from (Wüstholtz 2016).

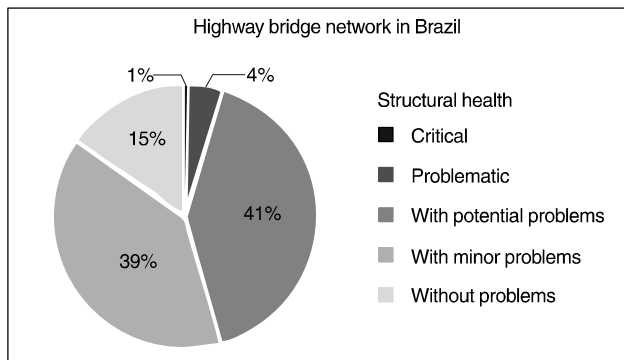


Figure 2. Structural health of the highway bridge network in Brazil.

Given that premise, the ability to monitor and maintain civil structures' integrity is a growing desire of bridge owners and managers (Jang et al. 2011; Farrar & Worden 2007; Spencer, Ruiz-Sandoval & Kurata 2004). Moreover,

many countries have enforced the maintenance of their infrastructure assets by constant updating their laws and regulations (Lehmann 2020), such as the German model building code (Argebau 2019), the German civil code, and the EU regulation for construction products (Europäisches Parlament, Rat der Europäischen Union 2011).

The successful practice of periodic visual inspection still predominates as the fundamental source of information in most maintenance programs (Li et al. 2016). A positive example is the German standard DIN 1076 for inspection and test of road infrastructures (DIN 1999), which its first version dates back to the '30s. Nonetheless, structural monitoring and maintenance programs' effectiveness depends on their required time to identify unsatisfactory performance (Brownjohn 2007). The early detection of structural damages can reduce the costs and deadlines associated with the maintenance of critical damages and provide better safety to the user public (Cho, Giles & Spencer 2015; Spencer et al. 2016).

Periodic visual inspection is limited to observations at discrete and distant points in time, and it is influenced by the inspector's subjectivity (Phares et al. 2013). Therefore, it fails to provide the full extent of structural health maintenance and user safety in civil infrastructures (Cho, Giles & Spencer 2015; Lynch 2007). Moreover, visual inspection procedures focus on visible physical damages, disregarding the safety and serviceability constraints adopted during the design phase. Hence, costly in-depth investigations and maintenance actions are often unnecessarily prompted based only on the visual perception of safety. Simultaneously, threatening events can occur between inspection appointments or undergo unnoticed for not being visible or accessible, such as the failure of prestressed tendons under certain conditions and risks from faulty execution. Only rare cases are the bridge maintenance actions triggered by a failed safety and serviceability check (Hajdin 2018). Therefore, visual inspections are inevitable as primary means of information but insufficient to satisfy the current needs for modern bridge maintenance programs and societal expectations (Lehmann 2020).

In this sense, structural health monitoring (SHM) techniques, i.e., deploying a sensor network with continuous data acquisition, robust data management, and intelligent data evaluation, have become increasingly sought (Jang et al. 2011). SHM systems have the potential to enable the implementation of real-time damage detection algorithms (Sakiyama, Lehmann & Garrecht 2021a) and the achievement of more realistic structural behavior and life expectancy through structural identification (Catbas, Kijewski-Correa & Aktan 2013) and finite element (FE) model updating methods (Sehgal & Kumar 2016).

1.2. Structural health monitoring of real-size concrete structures

Research efforts towards SHM of civil structures have increased substantially, with more than 17 thousand papers published in the last decade. However, most of these researches comprise laboratory tests with reduced-scale models in controlled environmental conditions and idealized failure modes (Cawley 2018). Only a few applications are present in real-size structures. The disappointing transfer rate of research to real-case application lies in the challenges of implementing a real-case SHM system, which is described in this section and summarized in Figure 3.

The main goal of an SHM system is to provide a reliable estimation of the actual structural health state and enable real-time detection of anomalous structural responses that could be related to damaging events. The number of sensors in real-size structures is, however, limited due to budget and logistic reasons (Sun & Büyüköztürk 2015), leaving a gap between measured information and structural response (Baquersad & Bharadwaj 2018). Therefore, SHM systems should be carefully designed to select the optimum number of sensing points and sensor layout to maximize the structure area coverage (Song, Lee & Eun 2021). The structural system also impacts the selection of sensing parameters and techniques. For example, in plane-trusses, nodal displacements can be estimated by measuring the axial deformation on selected truss elements (Xiao et al. 2017). That can be accomplished with point strain sensors, such as electric strain gages or local fiber optic (FO) strain sensors. On the other hand, the sensor's layout in a prestressed concrete bridge should prioritize the identification of tendon breaking and crack

formation at random locations. Therefore, SHM systems with distributed or quasi-distributed sensing and multiplexing, such as long-gauge fiber Bragg grating (LGFBG) deformation sensors, are more appropriated.

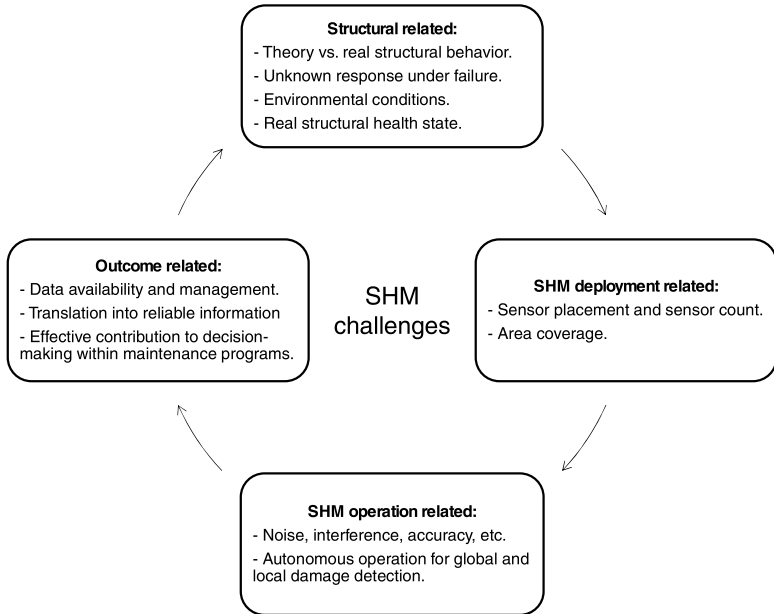


Figure 3. Main challenges in the deployment and operation of real-case SHM systems.

In laboratory tests or small monitoring deployments, engineers may evaluate the measured data and control the sensors' operation. In contrast, a high sensor-count SHM system that runs continuously should have an autonomous system capable of detecting anomalous signals during runtime (Sakiyama, Lehmann & Garrecht 2021a), followed by prognostic damage location and severity (Worden & Duluiu-Barton 2004). Moreover, the capacity to translate large amounts of data to reliable information – often disregarded in laboratory tests – still a present limitation in SHM deployments (Goulet & Smith 2013). As remote communication systems' availability increases and sensing technology becomes more and more accessible, the data stream of

SHM systems may become unmanageable. Many SHM operators report that they cannot handle such data volume, ending with piles of hard disks to store terabytes of raw data that no one will look at in detail (Cegla et al. 2011).

Moreover, a set of measured data alone is insufficient to assess a structure's actual condition, regardless of how good the sensing technology or how high the data availability (Sakiyama, Lehmann & Garrecht 2021b). Data interpretation strategies can be divided into model-based and data-driven methods (Catbas, Kijewski-Correa & Aktan 2013). Model-based methods rely on FE model predictions to quantify existing structural damages and identify new structural changes based on recent deviations. It typically operates by comparing measured data with FE simulation results, where an initial undamaged FE model is calibrated using model updating techniques that minimize the discrepancies between the simulated and measured structural response (Chen, Wu & Li 2018; Hou, Wu & Li 2018; Hong et al. 2015; Sanio et al. 2014; Okasha, Frangopol & Orcesi 2012; Ahrens et al. 2014; Krawtschuk et al. 2012). On the other hand, data-driven methods do not require information about the structural response. In this case, statistical parameters sensitive to structural changes (damage features) are calculated from the sensors' time series. Feature extraction methods such as the principal component analysis (PCA) and robust regression analysis are effective for long-term monitoring by keeping track of the damage features' changes in time and have been demonstrated in many laboratory and real-case applications (Laory, Trinh & Smith 2011; Zhang et al. 2015b; Posenato et al. 2010; Posenato et al. 2008).

Irrespective of the data interpretation method, acceleration-based modal identification, such as natural frequencies and mode shapes, is far the most common approach (Chen, Wu & Li 2018). Although highly sensitive to damage in homogenous structures, say steel structures and reduced models, natural frequencies lack the spatial resolution to detect local damage in real-scale concrete structures, and mode shapes are unreliable for large-scale SHM due to excessive noise (Hong et al. 2015; Cawley 2018). Indeed, Zhang et al. (2015a) reported that bridge engineers are increasingly losing their hopes on SHM systems as acceleration measurements fail to support bridge management's decision-making for being a too-global indicator.

As an alternative to acceleration-based measures, strain-based sensing can access structural response at a local level. Many applications using electromagnetic point-type strain gages are found in SHM for steel bridges (Ye, Su & Xi 2018; Catbas, Gokce & Gul 2012; Xu et al. 2011; Metzger & Huckelbridge 2009; Zhou 2006; Howell & Shenton 2006; Alampalli & Lund 2006). However, traditional strain gages are too local to monitor inhomogeneous material with random damage locations such as reinforced and prestressed concrete structures (Chung et al. 2008). Hence, strain-based sensing for SHM of inhomogeneous structures should be insensitive to material discontinuities at the micro and meso-levels but still enable measuring at the macro-level (Glisic 2011).

In this context, the long-gauge strain sensor using fiber-optic (FO) sensing is an alternative solution with great potential to fill in the gaps in the condition assessment of concrete structures and model updating techniques. With the recent development of long-gauge fiber Bragg grating (LGFBG) FO sensors for structural applications, it is possible to measure the average strain over the sensor's gauge, which can be customized regarding the structure's size, materials, and static behavior. Moreover, the FO sensing technology allows multiplexing, meaning that several sensors can be connected in series, creating a network for distributed strain measurements. Therefore, the SHM based on long-gauge sensors can measure the structure's global and local information, giving new opportunities for a reliable condition assessment of reinforced and prestressed concrete structures (Sakiyama et al. in press).

The design and operation of a real-size SHM for concrete structures is an extensive process. Engineers must thoroughly investigate issues related to the structural system, SHM deployment, SHM operation, and expected outcomes. The choice of sensing technique and sensor placement must be appropriate to extract relevant structural responses and detect possible failure modes. Moreover, intelligent algorithms for the autonomous operation and real-time detection of structural changes must be implemented to effectively complement regular periodic visual inspections. With such tools, bridge managers and inspectors have a reliable structural health assessment

between in situ inspections. Finally, a long-term real-size SHM system requires robust data management to translate thousands of terabits of measurement data into meaningful information to support bridge maintenance programs.

2. Aim and objectives

SHM of real-size concrete and prestressed concrete bridges based on fiber-optic (FO) sensing, with real-time damage detection capabilities and effective insertion into bridge maintenance programs, has not been widely reported. This research aimed to propose a long-term SHM concept to monitor prestressed concrete bridges, enabling the real-time detection of inherent damaging processes such as prestressing tendon break and crack opening and providing meaningful structural information to support decision-making within bridge maintenance. An SHM system based on long-gauge fiber Bragg grating (LGFBF) sensors was designed and deployed in a real-size prestressed concrete bridge. Autonomous and intelligent measurement tasks with data management and post-processing tools were implemented to operate the SHM system and deliver the expected results.

The research objectives were:

1. Investigate FO sensor technologies and select a suitable one to monitor prestressed concrete structures.
2. Design and deploy a long-term SHM system in a real-size prestressed concrete bridge.
3. Implement a data management system to handle the massive amount of measured data to make data access for structural evaluation feasible.
4. Develop a real-time algorithm for the detection of unexpected structural changes and reliable alarm triggering.
5. Build a 3D FE model to simulate the bridge's structural response under damaged scenarios.

6. Implement an integrated methodology to calibrate the FE model and estimate the bridge’s actual structural state using nonparametric post-processing analysis and Monte Carlo simulations.

This thesis is presented in a cumulative form. The objectives were divided into three peer-reviewed papers, where theory background, methods, and results are described in detail. Additionally, the original scripts developed during the research are available in an open-source data repository. Table 1 shows a summary of the publications and their respective scopes.

Table 1. Cumulative thesis: publication titles and their respective scopes.

N.	1	2	3	4
Title	<i>“Structural health monitoring of concrete structures using fibre-optic-based sensors: a review”</i>	<i>“A novel runtime algorithm for the real-time analysis and detection of unexpected changes in a real-size SHM network with quasi-distributed FBG sensor”</i>	<i>“Quantifying the actual damage level of a 60-year-old prestressed concrete bridge: a hybrid SHM approach”</i>	<i>“Data repository”</i>
Scope	Objectives 1. and 2.	Objectives 3. and 4.	Objectives 5. and 6.	Implemented scripts.

Section 3 describes the bridge structure where the SHM was deployed. The main structural issues and how the SHM system is expected to respond to such setups is summarized. The SHM conception and deployment are presented in Section 4. Section 5 shows the novel runtime algorithm for real-time analysis and detection of unexpected changes. Moreover, an overview

of the data management system is given. Section 6 presents the hybrid methodology for data interpretation and model updating. In Section 7, the original scripts implemented in this research are summarized. Lastly, the detailed information regarding the publications and their status at the thesis submission time is listed in Section 8.

3. B27 Bridge in Neckarsulm

The SHM deployment resulted from a cooperation between the Materials Testing Institute (*Materialprüfungsanstalt*, MPA), University of Stuttgart, and the Road Infrastructure Unit at the Stuttgart Regional Council (*Regierungspräsidium Stuttgart*, RPS). The RPS provided financial resources and a prestressed concrete bridge under their jurisdiction. In return, the MPA designed and deployed a pilot SHM system capable of detecting unexpected damage events, such as the rupture of tendons, and assessing the bridge's structural health.

The selected bridge was a prestressed hollow-core concrete bridge constructed in 1964. It is in Neckarsulm, Baden-Württemberg, Germany, belonging to the B27 state highway (Figure 4). It has three continuous spans with a constant width of 11.08 m with a total length of 57.0 m (17.0 m – 23.0 m – 17.0 m) without coupling joints. The two center columns are designed as individual supports with pot bearing. The superstructure is supported by two linear rocker bearings on the southern abutment, and the northern abutment, by two roller bearings. Figure 5 shows the bridge's longitudinal view, and Figure 6 its cross-section.

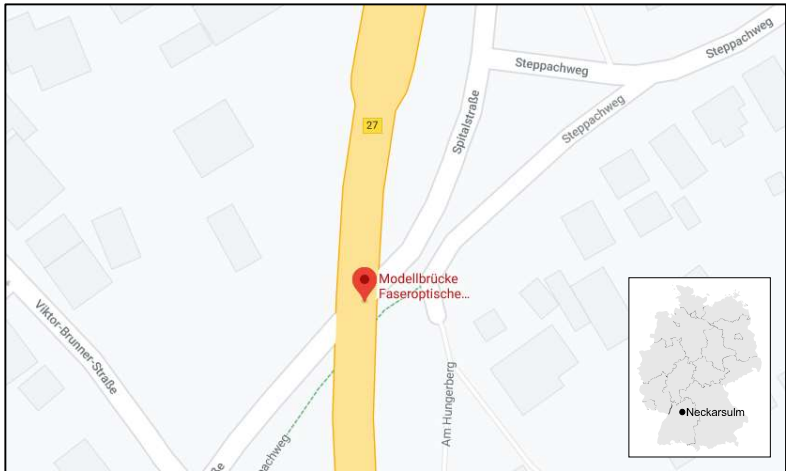


Figure 4. Map location of the B27 bridge in Neckarsulm, Germany (Geobasis-de 2021)

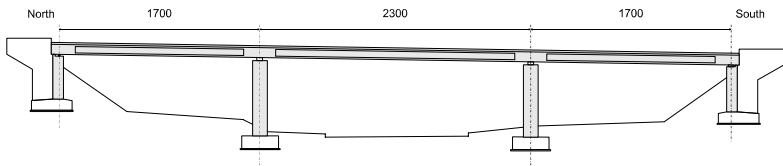


Figure 5. Longitudinal view of the bridge (dimensions in centimeters).

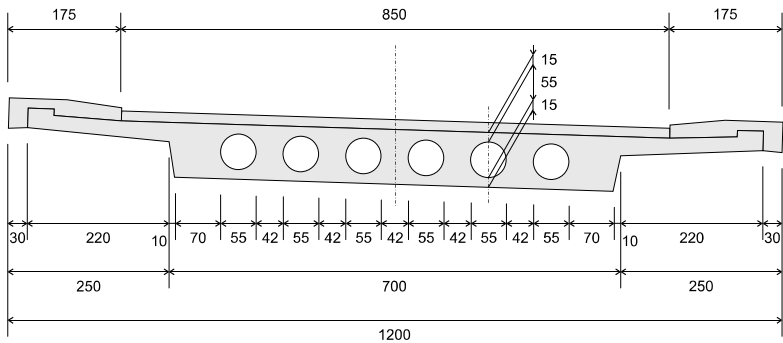


Figure 6. Bridge's cross-section (dimensions in centimeters).

The design load class is BK 60 (60 tons wheeled trainload), according to DIN 1072. Eighteen tendons span through the complete length, with an additional six tendons in the mid-span. Like many of the prestressed concrete structures designed and build until the '70s in Germany, the bridge has prestressing steel types of St 145/160 Sigma (tensioning methods KA141/40 and KA 35/10), which are known for their high vulnerability to stress corrosion-induced cracking (Ehman 2006). In addition to the high increase in traffic loads compared to the year of construction in 1964 and the corrosion-induced cracking risk, other critical problems may arise due to construction methods and the design standards adopted back then (Wüstholz 2016):

- Hollow-core bodies prevent two-axis load transfer and thus the redistribution of forces in the transversal.
- The temperature load case was not fully considered during the design process until the '80s, which can be critical to statically indeterminate structures, especially in combination with narrow webs and high slab slenderness.
- Shear forces were not considered to the extent that it is deemed necessary from today's standards. Minimum shear reinforcement was introduced only in 1967.
- Construction failures may already appear during construction caused by misplacement of the hollow cavities during concrete pouring and difficulties in compacting the surrounding concrete near the hollow cores.
- The hollow cavities cannot be examined as part of the regular visual inspections. Hence, inside damages and unaccounted loads, such as filling up with precipitation water, may not be detected in due time.

As part of DIN 1076 prescriptions, a construction book with the structure's technical information and records about inspection, repairs, and other relevant observations is available. Since the bridge's construction, inspections were periodically made as required. Since 2006, the bridge received a condition note of 3.0 on a scale from 1.0 to 4.0, as shown in Table 2.

Table 2. Structural condition classification according to DIN 1076 (DIN 1999).

Condition note	Classification
1.0 – 1.4	Very good structural condition.
1.5 – 1.9	Good structural condition.
2.0 – 2.4	Satisfactory structural condition.
2.5 – 2.9	Minimal structural condition.
3.0 – 3.4	Insufficient structural condition.
3.5 – 4.0	Inadequate structural condition.

In addition to the condition note, the bridge was deemed at risk of stress corrosion-induced cracking due to the adopted prestressing steel. From the static point of view, the structure is classified as collapse without announcement behavior given the small quantity of passive reinforcement steel adopted.

Therefore, an SHM system was proposed to detect tendon breaks in real-time and estimate the bridge's actual structural health state. The primary desired characteristic was a sensor technology with the appropriated spatial resolution and area coverage to detect random local damage formation and yet estimate the global structural response. Moreover, the SHM should be reliable for continuous operation and have robust data management to enable the effective transfer of the measured data to decision-making support. The next section describes the conception and deployment of the proposed SHM system.

4. Deployment of a fiber-optic-based SHM system

Traditional SHM approaches are based on single-point sensors with spatial resolution limited to a few millimeters. Sensors such as electromagnetic strain gauges, accelerometers, and inclinometers have been successfully analyzed in laboratory tests with many material types and deployed in SHM

systems of large structures with ductile and homogeneous materials, e.g., steel bridges (Mahadevan, Adams & Kosson 2014).

When it comes to reinforced concrete (RC) structures, their non-linear behavior, unknown crack formation locations, and material inhomogeneity challenge SHM systems' deployment. The limited number of feasible points to assess the structural behavior and the harsh environmental conditions compromise the successful monitoring of concrete structures using traditional point-type sensors (Kudva et al. 1993; Glisic & Inaudi 2012).

On the other hand, fiber-optic sensors (FOS) are characterized by their excellent sensitivity, durability, stability, and optimal installation size compared with traditional sensors. They are passive due to their dielectric construction and can bear high temperatures and harsh environments. The FO sensing technology can provide integrated, quasi-distributed, and truly-distributed measurements along with extensive measurement lengths (Lopez-Higuera et al. 2011). Thus, making them suitable for the long-term SHM of large structures requires comprehensive area coverage and local damage detection (Bao & Chen 2012; Li, Li & Song 2004).

Therefore, an extensive literature review was performed to understand the different FO sensing technologies' advantages, limitations, and drawbacks on SHM of concrete structures and subsidize the SHM conception for the selected bridge in Neckarsulm. The findings were published in the Magazine of Concrete Research (ICE), with the paper entitled "***Structural health monitoring of concrete structures using fibre-optic-based sensors: a review***" (Sakiyama, Lehmann & Garrecht 2021b).

4.1. Quasi-distributed fiber-optic sensors

Among the many FO sensing technic choices, the long-gauge fiber Bragg grating (LGFBG) strain sensors were deemed the most appropriated to meet the selected bridge's monitoring needs. The LGFBG sensors are classified as quasi-distributed FOS (Udd & Spillman 2011) due to their in-line multiplexing feature – where sensors are connected in series and measured in a single fiber array – combined with their long-gauge attribute. The structure's integral length, for example, can be monitored with distributed

yet discrete sensor arrays, hence the name “quasi-distributed”. The sensor’s gauge length determines the spatial resolution, which ranges from millimeters up to 10 m long (Wu et al. 2016), allowing the assessment of global information as well as local behavior to detect deflection and cracking in RC structures (Fouad et al. 2018; Wang, Jiang & Xiang 2018).

The fiber Bragg grating (FBG) allows the monitoring of global information (such as natural frequency) as well as local parameters (e.g., strain and deflection) in concrete structures (Fouad et al. 2018; Wang, Jiang & Xiang 2018). An FBG sensor consists of a microstructure with lengths varying from 5 to 10 mm (Udd & Inaudi 2005) with a sequence of evenly spaced etchings at a tuneable distance from each other carved with a UV laser in the core of a telecommunication FO (Huang et al. 2016). The light reflections at each etching are out of phase for most wavelengths, canceling the individual reflections due to the destructive interference. However, if a wavelength is harmonic to the etchings’ spacing, that wavelength’s reflections will be in phase, generating a constructive interference. Therefore, the reflected spectrum λ_B (or Bragg wavelength) will have essentially one wavelength corresponding to the etchings’ spacing (Giles & Spencer Jr. 2015; Iodice et al. 2005), as shown in Figure 7.

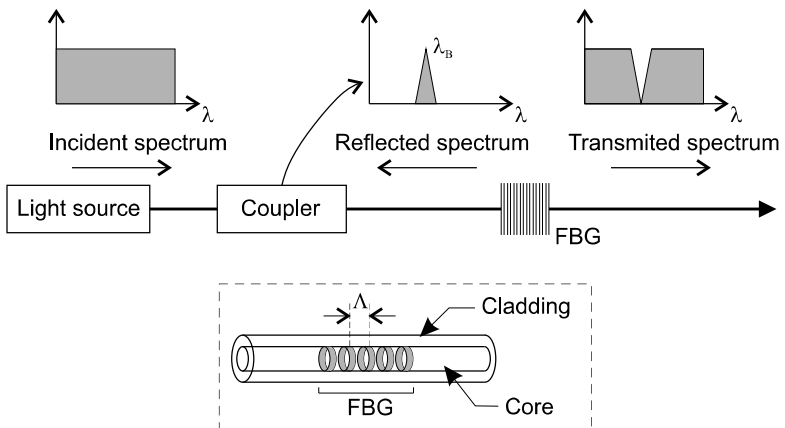


Figure 7. The measurement principle of the FBG sensor (adapted from Ye, Su & Han 2014)

The Bragg wavelength λ_B is given by:

$$\lambda_B = 2 \eta_{eff} \Lambda \quad (1)$$

where η_{eff} is the refraction index and Λ the grating period. The FBG as a sensing device is possible due to the linear relationship between the grating period and the Bragg wavelength (Giles & Spencer Jr. 2015). Thus, a Bragg wavelength variation due to external strain or temperature variation can be calculated by:

$$\Delta\lambda_B = \lambda_B [(\alpha + \xi) \Delta T + (1 - p_e) \Delta\varepsilon] \quad (2)$$

where $\Delta\varepsilon$ is the strain variation, ΔT the temperature change, α the coefficient of thermal expansion, ξ the thermotic coefficient, and p_e the strain-optic coefficient (Ye, Su & Han 2014).

The in-line multiplexing allows writing multiple Bragg gratings in a single FO cable or connecting a series of FBG sensors. If the specified wavelengths do not overlap, the interrogator unit can correlate the reflected spectra with each wavelength, as shown in Figure 8.

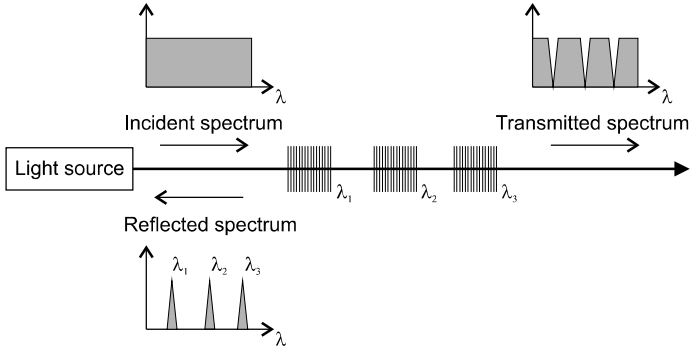


Figure 8. The in-line multiplexing of FBG sensors.

4.2. Long-gauge FBG sensors

The LGFBG sensing technology is known for its high sensitivity, durability, and stability. It can provide quasi-distributed measurements over extensive measurement lengths, making it appropriate for monitoring structures such as reinforced concrete and prestressed structures, where damage formation is usually local and random. Instead of measuring the strain of a single point of the structure, the long-gauge sensors can measure the average strain value along the sensor's gauge length, which can range from millimeters up to 10 m long (Wu et al. 2016), described as follows (Glisic 2011):

$$\varepsilon_{C,S} = \frac{\Delta L_s}{L_s} = \frac{u_B - u_A}{x_B - x_A} = \frac{1}{L_s} \int_{x_A}^{x_B} \varepsilon_{x,s}(x) dx + \frac{1}{L_s} \sum_i \Delta w_{d,i} \quad (3)$$

where $\varepsilon_{C,S}$ is the average strain along the sensor's gauge length; A, B are the sensor's anchoring points with coordinates x_A and x_B ; C is the sensor's midpoint; $L_s = x_B - x_A$ is the gauge length at the reference time; u_A and u_B are the x -axis component of displacements of points A and B after deformation is applied; ε_s is the average strain; $\varepsilon_{x,s}(x)$ is the strain distribution along the x -axis of the sensor; and $\Delta w_{d,i}$ is the dimensional change of the i th discontinuity, such as crack opening, dimensional inclusion change, etc., in the direction of the x -axis after the deformation is applied (Figure 9).

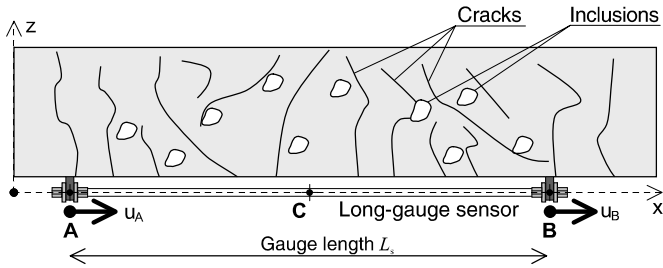


Figure 9. Representation of an LGFBG sensor surface mounted on concrete material (adapted from Glisic (Glisic 2011))

Glisic(Glisic 2011) published an extensive experimental trial to study the optimal gauge length to minimize the measurement error in inhomogeneous materials such as reinforced concrete. He provided design guidelines for the gauge length of prismatic beams subject to bending based on their static system (e.g., single span or statically indeterminate), load cases (e.g., distributed or concentrated forces), geometry (e.g., length, cross-section dimensions), and the likelihood of crack opening and spacing according to (Piyasena 2003). Especially when cracking occurs, the gauge length should be larger than the distance between cracks. Otherwise, the sensor will miss the crack opening and measure strain in the still tensioned concrete, which is much lower than the average strain in the beam, or measures the ratio between crack opening and gauge length, which does not represent the beam’s strain distribution (Glišić & Inaudi 2007). Since the typical spacing between cracks ranges between 100 and 300 mm (Piyasena 2003), a gauge length range is recommended between one and three meters (Glisic 2011).

The measurement error $\delta\varepsilon_{C,s}$ for a homogeneous material is calculated by subtracting the actual strain $\varepsilon_x(x_C)$ at the midpoint C from the measured average strain $\varepsilon_{C,s}$, as follows:

$$\delta\varepsilon_{C,s} = \varepsilon_{C,s} - \varepsilon(x_C, y_s) = \frac{1}{L_S} \int_{x_A}^{x_B} \frac{M(x)}{EI} y_s dx - \frac{M(x_C)}{EI} y_s \quad (4)$$

Glisic(Glisic 2011) defines simplified equations for different loading scenarios to estimate the maximum error for sensors “far enough” from the beam’s extremities. The errors are calculated as a function of the sensor’s gauge length, the beam’s length, the cross-section’s height, and the load’s case and position. Table 3 shows the estimated maximal errors for the sensors used in the SHM at the bridge in Neckarsulm, with a gauge length of 2.05 m. Three cases are considered for the side-spans and the mid-span: uniform distributed load, concentrated force, and a $w = 0.1$ mm crack opening. The calculated errors in Table 3 are a preliminary global indicator, and the detailed errors for each sensor will be discussed in the result section.

Table 3. Estimated measurement errors for the LGFBG sensors.

Position	Uniform distributed load	Concentrated force	Crack opening ($w = 0,1$ mm)
Side-spams ($L_{\text{beam}} = 17,0$ m)	0.50%	13.6%	12.7%
Mid-spam ($L_{\text{beam}} = 23,0$ m)	0.26%	10.1%	

4.3. The SHM system design

The proposed FO monitoring system is based on LGFBG strain sensors to continuously measure strain, temperature, and vibration at the bridge's superstructure. It consists of two parallel measuring lines, with 27 LGFBG sensors each, covering the bridge's total length, and five measuring lines with five LGFBG sensors in the transversal direction, all mounted on the superstructure's bottom surface. Additionally, ten LGFBG sensors are located on the main deck's sides to provide measurements in the longitudinal direction at a higher position, two accelerometers at the main deck's center, and four FBG temperature sensors. For every LGFBG sensor, an embedded FBG temperature sensor is present for temperature compensation.

A control cabinet was placed below the bridge at the southern side to accommodate an optical interrogator, an industrial computer for data acquisition, and an industrial LTE modem for data transfer. An FBG temperature sensor was placed inside the control cabinet to control the operating temperature. Sylex s.r.o manufactured the LGFBG sensors used in this project. (Sylex s.r.o 2021), and HBM FiberSensing S.A. the optical interrogator unit (HBM FiberSensing S.A. 2021). Figure 10 shows an overview of the sensors' layout. The cut A-A is depicted in Figure 11, and Figure 12 shows the sensor arrays' configuration and connections to the control cabinet. The 185 installed FO sensors are described as follows:

- strain in the longitudinal direction (sensors S01-S54 and S80-S89): for monitoring in the longitudinal direction, two quasi-distributed strain sensor lines are attached to the bottom of the bridge, located in the area of the prestressed cables (the sensors S80 to S89 were installed on the side of the structure at about 50 cm above the lower surface; the sensors S01 to S54 have a gauge length of 2.05 m, and the sensors S80 to S89 a gauge length of 0.50 m);
- strain in the transverse direction (sensors S55-S79): five strain sensor lines across the cross-section were installed on the underside of the bridge in the area of the maximum bending moments and on the two supports (these sensors have a gauge length of 1.35 m);
- temperature (sensors T01-T05): temperature sensors in the middle of the bridge, transverse to the direction of travel, and an additional temperature sensor inside the control cabinet;
- acceleration (sensors AC01-AC02): two accelerometers with a vertical measuring direction in the middle of the main field, underneath each driving lane.

The monitoring system in Neckarsulm has run continuously since November 2019 at a sampling rate of 200 Hz, generating over 70 thousand measurement points per second. The sampling rate was defined to optimize the representation of extreme values such as load peaks during a vehicle's crossing. Considering that the average travel-ing speed at the bridge is 60 km/h (and there are speed cameras a few meters from the north abutment), a sampling rate of 200 Hz provides an 8-centimeter measuring step. This enables extracting the complex dynamic behavior (e.g., peaks and strain influence lines) and characterizing the traffic load (vehicles' average velocity, the direction of travel, length, and the number of axles).

Additionally, the high sampling frequency was chosen to depict sudden events, such as the rupture of prestressed tendons, which is the core of the novel real-time analysis algorithm. However, the high sampling rate does not imply that all the measured data must be stored at the same pace. For

the novel damage detection algorithm, for example, the analyzed dataset rests in a temporary buffer. As soon as a batch of data is analyzed, only statistical results are stored. The raw data is then discarded, except if the algorithm detects an anomaly. In this case, only the affected data segment is completely stored (Sakiyama, Lehmann & Garrecht 2021a).

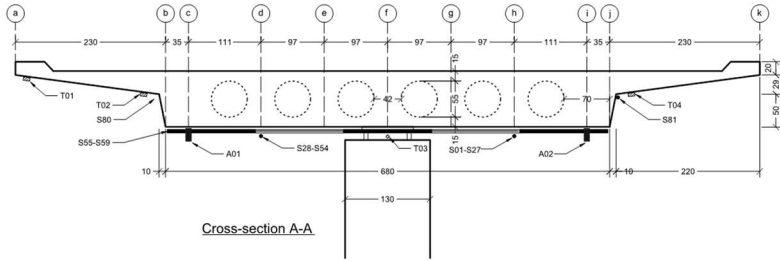


Figure 11. Cross-section A-A.

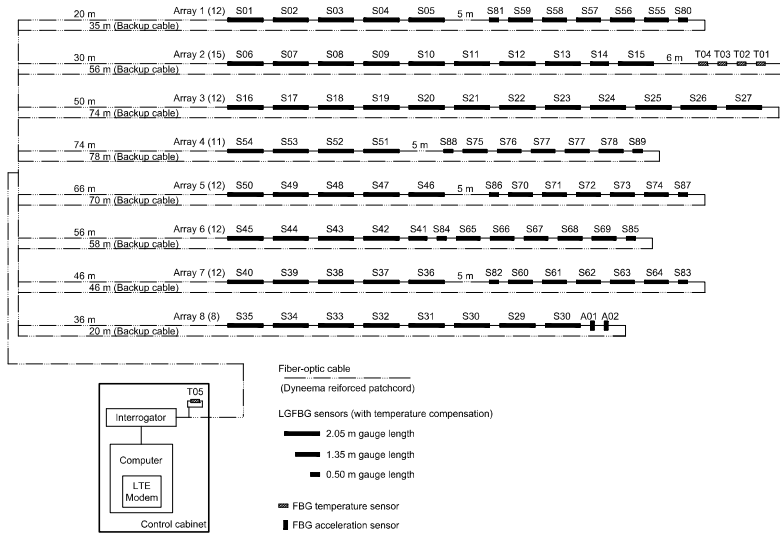


Figure 12. Sensor array configuration and control cabinet.

The LGFBG sensors were surface mounted using brackets screwed into the concrete using stainless steel hammer-set anchors EA II M8 from Fischer, with a length of 30 mm to prevent damaging the rebars and stirrups (the bridge's main deck has a concrete cover of 30 mm). The installation procedures were investigated beforehand in laboratory tests as part of a master dissertation (Fackler 2019) supervised by the author. Preliminary load

tests using FBG sensors are detailed in Fackler (2019) and Lehmann, Sakiyama & Fackler (2019).

The SHM system was deployed in 2019 for 12 days. Due to the high traffic volume on Spital street underneath the bridge, only a partial road closure was allowed. A mobile elevating work platform (MEWP) was used to allow the installation on the superstructure's bottom surface.



(a)



(b)



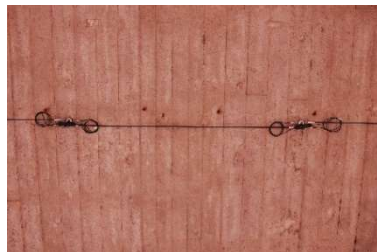
(c)



(d)



(e)



(f)



Figure 13. Overview of the bridge and SHM monitoring system: (a) overview of the bridge; (b) MEWP and partial road closure; (c) drilling works for the bracket’s fixation; (d) view of the quasi-distributed sensor’s lines; (e) view of installed sensors; (f) an LGFBG sensor with 2.05 m gauge; (g) view of the cabinet control installations; (h) detailed view inside the cabinet control.

4.4. Data management system

The monitoring system runs with a sampling rate of 200 Hz, generating 37,000 measurement points per second for the 185 installed sensors. Considering that each measurement point is a double-precision number, 16.4 Gigabytes of raw data are daily acquired. However, not all raw data needs to be stored and transferred. The temperature sensors used to compensate for the temperature influence at the LGFBG strain sensors, e.g., must be acquired with 200 Hz as the temperature compensation happens “online” but can be stored with slower frequencies. Even so, the data volume makes it unfeasible to deal with traditional worksheets and data-processing applications. Therefore, a big data approach based on multiple commercial software and original scripts was proposed to handle the large data sets and allow the raw data translation to meaningful structural information, as shown in Figure 14.

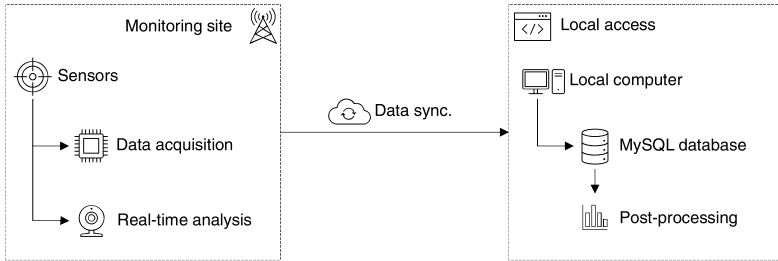


Figure 14. The big data management scheme.

The data acquisition is performed using the commercial software Catman AP developed and distributed by Hottinger Brüel & Kjaer (HBK). Catman is a robust acquisition software with tools design for the operation of long-term monitoring with high sensor-count, such as the online processing of computational channels and auxiliary channels that can be used to perform user-defined tasks via scripting. Moreover, the data acquisition process in Cataman (DAQ job) can be configured with multiple parallel recorders to, for example, store data from groups of sensors with different sampling rates. At the monitoring system in Neckarsulm, the following recorders were created and associated with a specific event:

- Dynamic triggered event (DT event): this event is triggered when a passing vehicle causes the derivate strain over time measured by the sensor located on the middle of the bridge to exceed $20 \mu\epsilon/s$. When activated, the event records all sensors (strain and temperature) 3 seconds before and 3 seconds after the triggering instance, capturing the vehicle's complete passage (considering traveling with a minimum speed of 34 km/h). The sampling rate is 200 Hz.
- Dynamic continuously event (DC event): all strain sensors are continually recorded at 200 Hz. The recorded data is saved in a new file every three hours. All the temperature sensors are parallel recorded every five minutes and saved separately every three hours.

- Statistical journal event (SJ event): a statistic journal stores the following values for all sensors every 15 minutes: maximum measured value, minimum measured value, and mean value.
- Real-time evaluation event (RT event): the statistical strain mode, the mean temperature, the maximal peak-to-peak strain amplitude, and the correlation coefficients for the strain sensors calculated during the real-time evaluation script are stored. The values are recorded every minute.

Once stored at the monitoring site, the data is transfer via cloud data synchronization to a local computer. The original scripts wrote in MATLAB (MATLAB 2020) are responsible for data cleansing, data extraction, permanent storage in a MySQL (*MySQL Workbench 8.0* 2020) database, post-processing, and result representation. More information about the proposed data management system can be found in the paper “*A novel runtime algorithm for the real-time analysis and detection of unexpected changes in a real-size SHM network with quasi-distributed FBG sensor*”, published in Sensors journal (Sakiyama, Lehmann & Garrecht 2021a).

5. A novel runtime algorithm for the real-time detection of unexpected structural changes

The real-time detection of structural damage is the utmost desired level of sophistication in an SHM system. With real-time information, actions can be promptly taken to avoid life-threatening consequences. The detection of structural changes in real-time is usually performed with data-driven methods that use nonparametric, baseline independent, and statistical learning approaches to extract intrinsic structural features without requiring prior knowledge of the structure health (Santos et al. 2015; Santos et al. 2016; Cremona & Santos 2018; Kim et al. 2019; Lydon et al. 2021).

Still, those concepts of the real-time capability to detect structural changes are only feasible to a limited extent. That’s because damage detection is usually performed after a data set is stored, possibly transferred to a local computer, and analyzed by a third-party algorithm. Although this process may not require human interference, damage detection depends on a combination of tasks performed in different places with different computational tools. For example, if a dataset is corrupted, remote data synchronization fails, or the operating system that performs the data analysis is down, the real-time detection of structural damages fails.

Therefore, a new concept of real-time damage detection was proposed in this research. User-defined tasks were implemented via original scripts inside Catman acquisition software. The measured data is analyzed during runtime, i.e., as soon as measurement values are generated and even before data storage occurs. The novel runtime algorithm relies on a three-step check based on different structural parameters to deliver a reliable alarm triggering system.

The detailed literature review, method description, and results from the novel runtime algorithm for real-time damage detection were published in the journal *Sensors* (Mdpi), with the paper entitled “***A novel runtime algorithm for the real-time analysis and detection of unexpected changes in a real-size SHM network with quasi-distributed FBG sensor***” (Sakiyama, Lehmann & Garrecht 2021a). The novel algorithm’s theoretical background was extracted from (Sakiyama, Lehmann & Garrecht 2021a) and is presented as follows.

In the proposed runtime algorithm, statistical values are continuously updated from the strain and temperature data stream of each sensor over an optimized n -sampled moving time window τ_n , namely the statistical strain mode M_0 , the arithmetic strain mean μ , the arithmetic temperature mean \bar{T} and the maximal peak-to-peak amplitude u . Additionally, the strain data from the time window τ_n for every two adjacent sensors p and q are analyzed, where the correlation coefficient $\rho_{pq}(\tau_n)$ for the measured strain $s_p(k)$ and $s_q(k)$ are calculated according to:

$$\rho_{pq}(\tau_n) = \frac{\sum_{k=1}^n (s_{p,k} - \mu_p) \cdot (s_{q,k} - \mu_q)}{\sqrt{\sum_{k=1}^n (s_{p,k} - \mu_p)^2} \cdot \sqrt{\sum_{k=1}^n (s_{q,k} - \mu_q)^2}} \quad (5)$$

For a continuous monitoring system with high sampling rate measurements on coherent structures with consistent loading, the correlation coefficient between a pair of sensors must remain constant and close to one, if they are well correlated or close to zero, if there is no correlation. In the case of adjacent sensors disposed along the longitudinal direction of a continuous beam, the correlation coefficient should remain stationary and close to one until a change occurs in the structural system (Catbas, Gokce & Gul 2012). The evaluation of the correlation between two sensors can also be used to infer already existing geometric discontinuities, e.g., hollow bodies or built-in parts or pre-existing damages in the structure.

Although the correlation coefficient is a relevant parameter, it cannot be used alone as an indicator of structural change since noise and influences from wind or traffic loads, amongst others, can also lead to deviations in the correlation. Therefore, the implemented algorithm is based on a three-step validation to avoid false calls and enhance its reliability. Should the correlation coefficient for two correlated sensors drop below a pre-defined threshold within the time window τ_n , the maximal peak-to-peak amplitude u and the strain-offset through the statistical strain mode Mo of both sensors during τ_n are examined. Under normal operation conditions, the peak-to-peak amplitude is directly related to the traffic load. Simultaneously, the statistical mode represents the strain signal offset due to the environment temperature variation and can be considered the “unloaded state” of the bridge for a short time window.

Suitable limit values must be defined for all three indicators. The correlation coefficient threshold is set as 0.9, a relatively low value considering the observed measurement history for one year. Since no load test was performed on the monitored bridge, the peak-to-peak amplitude limit was taken from the cumulative distribution plot of the maximal observed values for the sensors located at the middle of the bridge and set as 60 $\mu\text{m}/\text{m}$. The

strain offset is defined by observing the statistical strain mode of short moving time-windows τ_n over a long measuring period. Since the strain sensors are temperature compensated, and the bridge superstructure is free to deform in the longitudinal direction, the statistical mode values' changes are mainly due to the structural deformation due to the temperature variation. A linear correlation between the strain mode and the temperature can be observed, with a statistical variation coefficient of one and an inclination of $12.82\text{e-}6$ °C. Therefore, an abrupt non-linear behavior between the strain mode and the temperature variation indicates an unexpected event unrelated to temperature changes, such as a crack opening or a change in the static behavior.

Figure 15 shows the three-step check for alarm triggering present in the novel runtime algorithm for real-time damage detection, where ρ is the correlation coefficient, u_i is the peak-to-peak strain amplitude, $\Delta M o_i$ is the statistical strain mode variation, and ΔT is the average temperature variation. For more details, refer to Sakiyama, Lehmann & Garrecht (2021a).

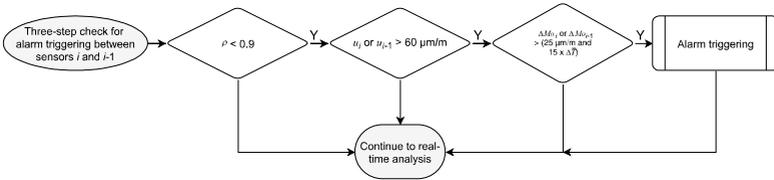


Figure 15. Three-step check for alarm triggering flowchart (Sakiyama, Lehmann & Garrecht 2021a).

In contrast to the traditional alarm triggering approaches, the monitoring system in Neckarsulm does not rely on absolute or singular thresholds. Each derived parameter is particularly sensitive to different factors: the statistical strain mode to the temperature influence, the peak-to-peak strain amplitude to the traffic load, and the correlation coefficients to the static system behavior. Only if the three indicators individually show critical values, an alarm is triggered, allowing the bridge managers to evaluate all three indicators together with the complete measurement data from all sensors.

6. Damage identification and FE model updating

Damage detection in the context of SHM programs is usually performed in two ways: with model-based or data-driven methods (Catbas, Kijewski-Correa & Aktan 2013). Model-based methods use calibrated FE models to estimate the structural health actual state. The so-called FE model updating process correlates simulated FE results with measured values and applies corrections in the FE model properties to optimize the discrepancy between simulated and measure values (Krawtschuk et al. 2011; Strauss et al. 2012; Strauss et al. 2011; Chen, Wu & Li 2018; Hou, Wu & Li 2018; Hong et al. 2015; Sanio et al. 2014). Existing damages can be quantified, and new structural changes identified based on new deviations. However, model-based approaches are time-consuming and demand high computational costs. Given the many uncertainties in a real-size structural system, the calibrated model may behave erroneously even if the simulated results match the measured values (Goulet, Kripakaran & Smith 2010).

Data-driven approaches dismiss information about the structural physical response. Instead, statistical parameters sensitive to structural damages are extracted from the sensors' dataset, for example, using nonparametric feature extraction such as the principal component analysis (PCA) and robust regression analysis (Zhang et al. 2015b; Posenato et al. 2010; Waibel et al. 2018; Zhang et al. 2015a; Laory et al. 2013; Zhu et al. 2019). They are effective for long-term monitoring as they keep track of the statistical parameters' changes in time. However, existing structural damages are more complex, if not unfeasible, to detect.

Irrespective of the method, damages are usually attributed to structural elements at or near a sensor that display abnormal behavior. This assumption is realistic for statically determinate structures, given that the distribution of internal forces is insensitive to stiffness changes. Hence, a statically determinate beam's internal forces, e.g., remain unaltered if a segment suffers a stiffness reduction, changing only deformations at the affected part. On the other hand, in statically indeterminate structures, the internal forces are redistributed every time a segment's stiffness changes.

Consequently, the source of a sensor’s inconsistent behavior may be damage formation at its location, or a combination of damages dispersed in the structure. Thus, real-size SHM systems should be designed with appropriate sensor-count, area coverage, and optimized placement to evaluate the damage distribution correctly.

To cope with those challenges, a hybrid methodology to quantify the actual structural damage level was proposed. The novelty consists of combining data-driven and model-based methods for the calibration of an FE model and structural damage estimation based on the LGFBG sensors’ strain history. The methodology’s core is the strain feature extraction using the principal component analysis (PCA) method, which is performed for both the dynamic strain history from the SHM system and the FE model simulation results. Additionally, complementary tasks, namely traffic characterization, sensitivity analysis, Monte Carlo simulation, and objective function optimization are implemented in the proposed integrated methodology.

The detailed literature review, method description, and results from the integrated methodology for data interpretation and model updating were submitted to the journal Structural Health Monitoring (Sage), with the paper entitled “*Quantifying the actual damage level of a 60-year-old prestressed concrete bridge: a hybrid SHM approach*” (Sakiyama et al. in press). The theoretical background for the PCA method and the traffic characterization tasks are described in sections 6.1 and 6.2.

6.1. PCA method

The principal component analysis theoretical background was extracted from Sakiyama et al. (in press) and is presented in this section.

The principal component analysis (PCA) is a quantitative method used to simplify multivariate statistics problems by replacing the original data with a new set of variables that still contains most of the information, called the principal components (*MATLAB* 2020). The principal components have no physical meaning, but they describe the directions that explain a maximal amount of variance, i.e., the axes that provide the best angle to see and eval-

uate the data. The first principal component is composed of the axes' directions that capture each variable's largest possible variance. The second principal component is another set of axes perpendicular to the first and accounts for the next highest variance. This process continues until the number of calculated principal components equals the number of variables in the original data. The complete set of principal components is a square matrix of order n , where n is the number of variables. However, it is commonplace that the first few principal components explain over 80% of the total variance. Therefore, they can be used to understand the driving forces that generated the original data (Jaadi 2019).

The principal components are constructed by calculating the eigenvectors and eigenvalues of the data's covariance matrix. The eigenvectors represent the axes' direction with the most variance, while the eigenvalues are coefficients that give the amount of variance carried by each eigenvector. The principal components are simply the eigenvectors sorted in order of their eigenvalues.

First, a matrix with the strain histories from selected sensors is constructed for the analyzed time window τ_n , where the result is an N by n matrix:

$$S(\tau_n) = \begin{pmatrix} S_i(t_j) & \cdots & S_N(t_j) \\ \vdots & \ddots & \vdots \\ S_i(t_{j+n-1}) & \cdots & S_N(t_{j+n-1}) \end{pmatrix} \quad (6)$$

with $i = 1$ to N and $n = \text{size}(\tau_n)$

where N is the number of sensors, j is the first sample in the time window τ_n , and n is the time window's size in samples. Since the PCA is sensitive to the initial variables' variances, the resulting matrix must be normalized to assure that they contribute equally to the analysis. Each variable is centered on having a mean of 0 and rescaled to have a standard deviation of 1. The normalized matrix s of the strain history is given as

$$s = \begin{pmatrix} S_i(t_j) - \overline{S_i(\tau_n)} & \cdots & S_N(t_j) - \overline{S_N(\tau_n)} \\ \vdots & \ddots & \vdots \\ S_i(t_{j+n-1}) - \overline{S_i(\tau_n)} & \cdots & S_N(t_{j+n-1}) - \overline{S_N(\tau_n)} \end{pmatrix} \quad (7)$$

where $\overline{S_i(\tau_n)}$ is the mean value for the sensors' strain history during τ_n . Next, the covariance matrix $C(\tau_n)$ for all measured samples is constructed from the standardized matrix s as follows:

$$C(\tau_n) = \begin{pmatrix} cov(s_1, s_1) & \cdots & cov(s_N, s_1) \\ \vdots & \ddots & \vdots \\ cov(s_1, s_N) & \cdots & cov(s_N, s_N) \end{pmatrix} \quad (8)$$

with $cov(s_p, s_q) = \frac{1}{n-1} \sum_{k=1}^n (s_{p,k} - \mu_p) * (s_{q,k} - \mu_q)$,

p and $q = 1$ to N

where μ_p is the mean of the data series s_p , μ_q the mean of the data series s_q , and $*$ denotes the complex conjugate. Finally, the eigenvalues λ_i and eigenvectors Ψ_i of the covariance matrix are obtained by satisfying the equation $[C(\tau_n) - \lambda_i I] \Psi_i = 0$, for $i = 1$ to N .

When the eigenvectors are sorted by their eigenvalues in decreasing order, they are arranged in order of significance, resulting in a $N \times N$ matrix, also called the principal components (PC) matrix, where N is the number of variables. The first few eigenvectors' columns contain most of the original data variance information, as explained before. They can be used to understand how each variable contributes to the overall behavior and how they interact.

6.2. Identifying and classifying heavy vehicles' crossing

An important task to assure the damage identification model updating reliability is to characterize the load cases that will be assessed. For a bridge structure, it is reasonable to consider the crossing of a single heavy vehicle as to the most representative external load. However, vehicles with different velocities, weights, lengths, and axle numbers cross the bridge at a random pace. Moreover, multiple heavy vehicles may cross the bridge simultaneously

and in opposite directions. Therefore, post-processing scripts were developed to identify when a single vehicle crosses the bridge and categorize the recorded vehicles' crossing about their number of axles, total length, and travel direction. Representative load cases were then defined from the categorized traffic information. The process for identifying and classifying heavy vehicles' crossing is described in this section.

The SHM at the Neckarsulm bridge does not have a weight in motion (WIM) or similar system to identify the vehicles' weight and axle number. Therefore, a triggered event assesses the dynamic strain changes over time to detect a heavy vehicle's crossing. The event is triggered if the derivative strain over sample measured by either of the two sensors located at the bridge's midpoint exceeds $10 \mu\epsilon/100$ samples, which is equivalent to $20 \mu\epsilon/s$ at 200 samples/s. The $20 \mu\epsilon/s$ threshold was established based on observation. Only the maximum peak-to-peak amplitude cases at the bridge's midpoint bigger than $20 \mu\epsilon$ are recorded as a practical result. A pre-trigger buffer stores the data from all sensors for a three-second moving time window (600 samples). When triggered, the event records the next three seconds for all sensors (strain and temperature) and appends them to the pre-trigger buffer. The final six seconds of measurement (1,200 samples) are stored in a separate file and later uploaded into the project's SQL database. The six-second measurement should capture the complete vehicle's crossing, considering traveling with a minimum average speed of 34 km/h. Between December 2019 and February 2021, over 60 thousand vehicles' crossings were recorded. Figure 16 shows, for example, the strain history recorded during the crossing of a heavy vehicle on 10 December 2019. Only sensors S01 to S27 (located underneath the driving lane in the northern direction of travel) are plotted, and sensors S01 and S27 are highlighted.

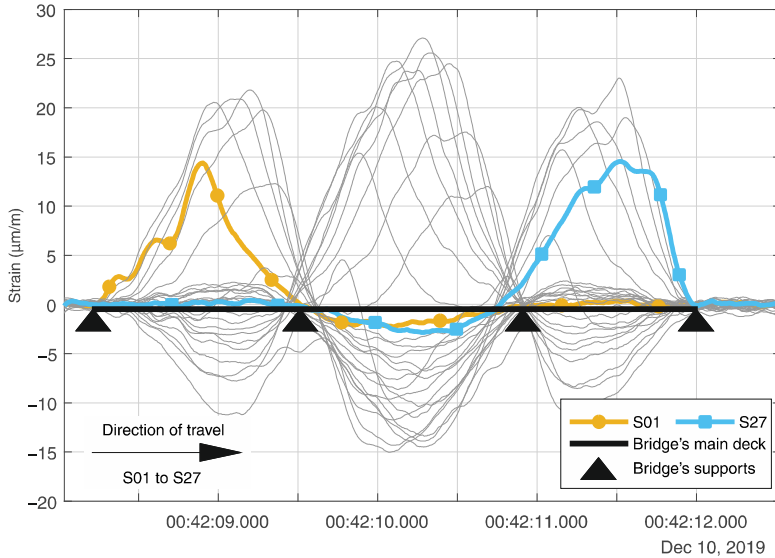


Figure 16. Strain history for sensors S01 to S27 during the crossing of a heavy vehicle. The data has a length of 1,000 observations (5 seconds). The abutments' approximated position and the intermediary columns are represented with triangles, and the bridge's main deck is depicted as a thick horizontal line. The strain lines for sensors S01 and S27 are highlighted. The other strain lines are shown in grey.

The cross-covariance function is applied between selected pairs of sensors to estimate the vehicle's velocity. The cross-covariance is a powerful tool to measure the similarity between time series in signal processing. It calculates how much one signal must be shifted in time (also referenced as lag) to become comparable to the other. Consider two identical sine waves, e.g., that are out of phase. Using the cross-covariance function, one can calculate the phase difference in terms of samples between the two signals without knowing their equations. The sine wave example is simple since all points in the time series have the same phase difference.

However, the cross-covariance function also allows the time shift calculation of each time-point in stochastic processes. Take sensors S01 and

S27, for example, highlighted in Figure 16. Considering the northern direction of travel, S01 is the first sensor and S27 the last crossed by the vehicle. Since the bridge geometry and the sensors' placement are symmetric about the bridge's center, S01 and S27 strain histories have the same global behavior but are mirrored about the time. Both sensors will record the maximal strain when the vehicle's center of mass is located at the sensor's position. Therefore, as soon as the vehicle enters the bridge, sensor S01 measures its maximal strain. The same happens with sensor S27 as the vehicle is about to finish the crossing. Applying the cross-covariance function, one estimates how much each sensor S27 point must be shifted to the right to be as similar as possible to the sensor S01 signal. The shift can also be used to determine the direction of traffic. If sensor S27 shift regarding sensor S01 is negative, travel direction is from S01 to S27. But, if the S27 shift is positive, the travel direction is from S27 to S01.

Additionally, the cross-covariance is used to detect if more than one heavy vehicle simultaneously crossed the bridge in opposite directions. The hypothesis that the strain history from two sensors equidistant from the bridge's midpoint is symmetric is only valid if a single heavy vehicle crossed the bridge. Therefore, if the cross-covariance returns a function whose form is unrelated to the original strain history behavior, it is likely that more than one heavy vehicle crossed the bridge. In that case, the recorded event is excluded from the analysis.

Since the maximal strain from both sensors happens when the vehicle is at each sensor's location, the shift between the sensors' maximal values can be considered as the duration of travel between them. If the distance between the two sensors and the measurement sampling are known, the average velocity between their locations can be calculated. Table 4 shows the average velocity estimated from two sensors equidistant from the bridge's center during the vehicle crossing recorded in Figure 16. The average speed was 19.42 m/s or 0.0971 m/samples.

Table 4. Average velocity estimated with the cross-covariance function from the strain history in Figure 16.

Pair of sensors	Distance between sensors' midpoint	Maximal strain's shift (lag)	Average velocity
S01 and S27	51 m	519 samples (2.595 s)	19.65 m/s (70.7 km/h)
S02 and S26	47 m	490 samples (2.45 s)	19.18 m/s (69.0 km/h)
Average			19.42 m/s (0.0971 m/samples)

Once the average velocity is known, the vehicle's length, number of axles, and distance between axles can be estimated from the first sensor's signal in the travel direction. Figure 17 shows the sensor S01 strain history at the beginning of the vehicle's crossing extracted from Figure 16. Since the distance between the bridge's abutment and sensor S01 anchoring is two meters (inferior to the average axle distance for heavy trucks), it is possible to identify when each axle, or at least each group of axles, entered the bridge. It is assumed that the maximal strain value in sensor S01 happens when the last group of axles reaches the sensor's midpoint. Therefore, the segment between the first sample and the maximal strain value is analyzed. The local maximums and minimums are identified by the changes in the strain signal's gradient. If the strain gradient turns positive, it indicates that an axle has entered the bridge and the strain grows as it travels towards the sensor. If the strain gradient changes to negative, the axle reaches the sensor, and the strain reduces as the axle leaves the sensor. During the vehicle's crossing shown in Figure 16, the strain gradient changed six times, as shown in Figure 17. Figure 18 shows the estimated vehicle's position for each of the six marked gradient changes.

Finally, the distance between axles or groups of axles is calculated by computing the distance in samples between the positive gradient changes and multiplying it by the vehicle's average velocity in meters per sample. Table 5 shows each positive gradient change location at samples 44, 81, 120, and 134 and the respective distances in samples and meters. All the sample

locations in Table 5 are depicted in Figure 17, except sample 120. That location was not represented in the graphic due to scaling, given that it is too close to location 134. Figure 19 shows the interpretation of the estimated axle in Table 5 distance in a fictitious truck. It is worth mentioning that identifying the first axle at sample 44 and the last at sample 134 happened in 0.45 seconds.

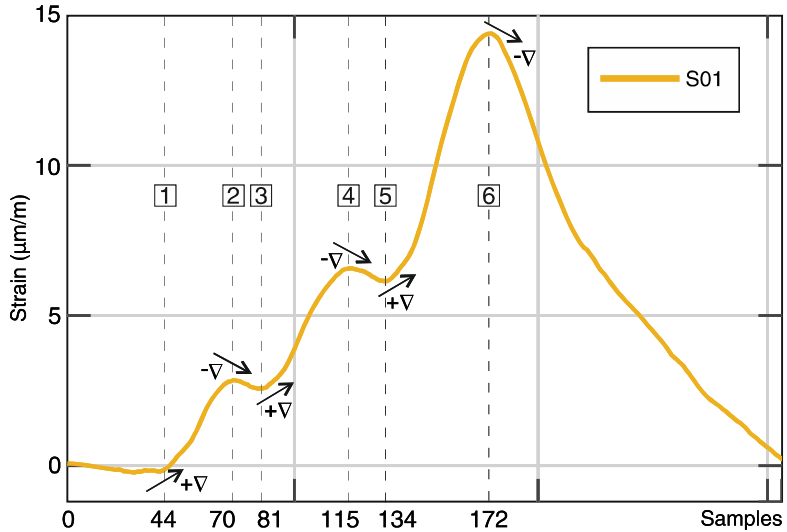


Figure 17. Sensor S01 signal at the beginning of the vehicle’s crossing in Figure 16. The local maximums and minimums (gradient changes) are marked with a vertical dashed line and numbered from 1 to 6.

The same analysis is performed for the southern direction but with sensors S28-S54 located underneath the southern driving lane. The average velocity is calculated with the cross-covariance between sensors S28 and S54. The vehicle’s number of axles, the distance between axles, and total length are estimated from sensors S54 signal, the first sensor in the southern direction of travel.

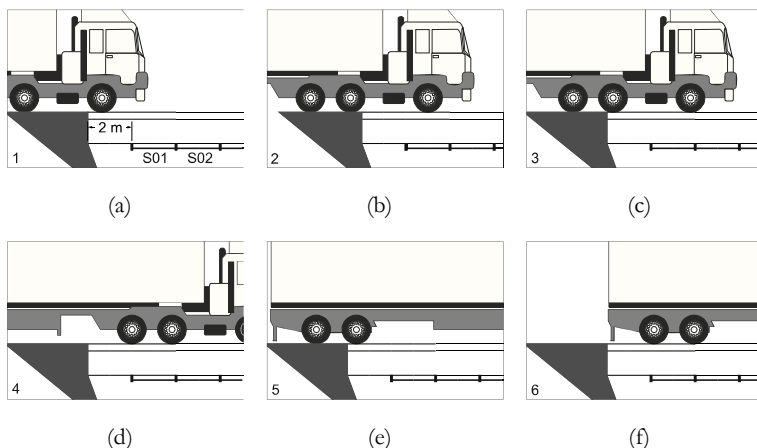


Figure 18. Axles' estimated position during the vehicle's entrance at the bridge. Each figure corresponds to a dashed vertical line in Figure 17: (a) the front axle enters the bridge at sample 44. The strain gradient is positive; (b) the Front axle reaches sensor S01 at sample 70 and moves forward to sensor S02 before the second axle has entered the bridge. The strain gradient is negative; (c) the second group of axles enters the bridge at sample 81. The strain gradient is now positive; (d) the second group of axles reaches sensor S01 at sample 115 and moves forward to sensor S02. The strain gradient is again negative; (e) the last group of axles enters the bridge at sample 134. The strain gradient is positive; (f) the last group of axles finally reaches sensor S01 at sample 172.

Table 5. Estimated axle distances.

Positive gradient change locations (samples)	Distance (samples)	Distance (meters)
44	-	-
81	37	3.6 m
120	39	3.8 m
134	14	1.4 m
Approx. vehicle's length		8.8 m

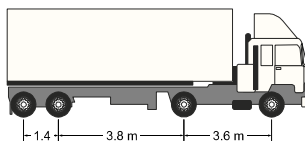


Figure 19. Axle distances representation.

The steps described above were applied to the over 60 thousand recorded crossings. The following targets were set to select the characteristic crossings and avoid inaccurate measurements:

- The crossing of a single heavy vehicle (in either direction);
- Number of identified axles equal or higher than 2;
- Average velocity smaller than 30 m/s (108 km/h);
- Maximal strain at the bridge's midpoint higher than 20 $\mu\text{m}/\text{m}$.

From the over 60 thousand recorded crossings, 11,470 were within those constraints. Figure 20 shows the characterization of the selected vehicles' crossing. Figure 20.a displays the percentages of vehicles in the direction of travel. The northern direction means that the vehicle crossed at the driving lane where sensors S01 to S27 are located, and the southern direction at the driving lane with sensors S28 to S54. From 11,470 crossings, 8,029 (70%) were in northbound, and 3,441 (30%) in southbound. Figure 20.b to Figure 20.d show the density normal distribution plot for the average velocity, axle number, and maximal measured strain, which have mean values of 18.4 m/s (66 km/h), 4 axles, and 30.2 $\mu\text{m}/\text{m}$, respectively. For the vehicles' length, the plots were divided into vehicles up to 6.5 m long (Figure 20.e), and vehicles longer than 6.5 m (Figure 20.f), with mean lengths of 4.6 m and 9.8 m.

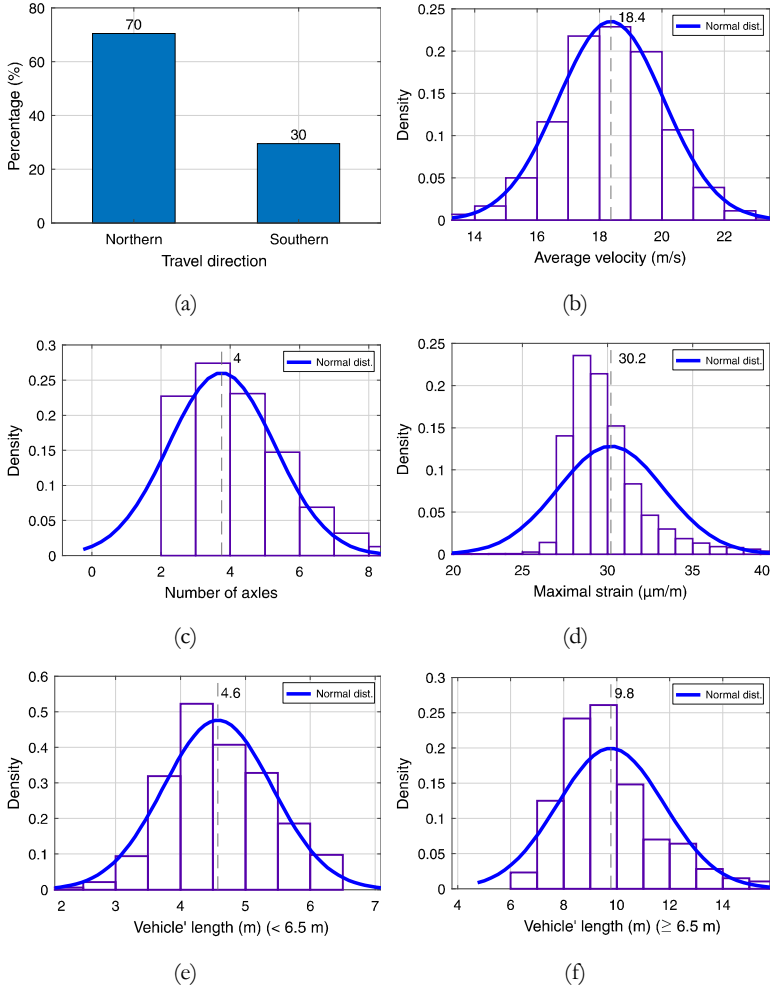


Figure 20. Characterization of heavy vehicles' crossing. The normal distribution mean values are represented with a dashed line and the respective value at the top: (a) Direction of travel; (b) Average velocity; (c) Number of axles; (d) Maximal measure strain; (e) Vehicles' length up to 6.5 m; (f) Vehicles' length from 6.5 m.

7. Implemented scripts

This research’s methodology was executed using original scripts written by the author. This section presents a summary of the developed scripts according to their related role. All 47 scripts, with over 250 pages and 11,000 code lines, were used during the research for data management, analysis, result generation, and result representation. The original scripts were published in a data repository and can be accessed from Sakiyama (2021). The tables are organized as follows:

- Table 6 – Data storage-related;
- Table 7 – Novel runtime algorithm for rea-time damage detection related;

Table 8 – Dynamic event-related;

- Table 9 – PCA related;
- Table 10 – FE model-related;
- Table 11 – Rainflow analysis related;
- Table 12 – Statistical strain mode and temperature related.

Table 6. Data storage related.

Pos.	Script name	Input argument	Output argument	Description	N° code lines
1	createCoeffDB	-	-	Create SQL tables to store the sensors' calibration coefficients.	43
2	createCorrDB	-	-	Create an SQL table to store the real-time	97

				algorithm's results	
3	createRecorderDB	-	-	Create SQL tables to store the dynamic triggered event results.	219
4	createStatDB	-	-	Create SQL tables to store the statistical journal's results.	676
5	loadCoeffDB			Load the sensors' calibration coefficients to the SQL table	61
6	loadCorr	-	-	Load the real-time algorithm's results to the SQL tables.	389
7	loadRecLongRF	-	Rainflow analysis results	Read raw data from the continuous dynamic event and performs the rainflow analysis for the strain signals.	313
8	loadRecShort	-	-	Read raw data from the dynamic triggered	444

				event and load them to the SQL database.	
9	loadStat2	-	-	Read raw data from the statistical journal and load it to the SQL database.	370

Table 7. Novel runtime algorithm for real-time damage detection related.

Pos.	Script name	Input argument	Output argument	Description	N° code lines
10	colect_coef	Sensors' name and threshold values.	Structure with results.	Create a structure with the real-time algorithm's results accordingly to the input arguments and plot the box plots with the three-step check results.	564
11	show_correlation	Called from call_show_correlation.	Strain signals and timestamp.	Plot the time-windows related to the strain history for a case where	140

				the three-step check was triggered.	
12	call_show_correlation	Structure with results from collect_coeff and index case.	Strain signals and timestamp.	Prepare data and set parameters to call show_correlation.	50

Table 8. Dynamic event related.

Pos.	Script name	Input argument	Output argument	Description	N° code lines
13	readDataShort	SQL file_id, SQL table name, and plot configurations	Sensors' signal for the dynamic triggered event.	Retrieve a dynamic triggered event from the SQL database and plot the results accordingly to the plot configuration input.	1054
14	colect_corr_short	SQL table name.	Structure with the correlation coefficient's results.	Collect the correlation coefficient results from all vehicles' crossings (6-second measurements) in the SQL database.	148

15	v_dir	-	Structure with traffic statistics.	Get traffic statistics from all dynamically triggered events in the SQL database, namely: travel direction, average velocity, axle number, vehicle's length, maximal strain, mean temperature, and timestamp.	57
16	cross_corr	Strain histories from a dynamic triggered event.	Traffic statistics from a dynamic triggered event.	Subroutine	96
17	get_traffic	Structure with traffic statistics.	Filtered traffic statistics in table format.	Filter the structure with traffic statistics about the minimum average velocity and number of axles. Return the results in table format for plotting.	38
18	plot_travel_stat	Traffic statistics in	-	Bar plot of the travel	44

		table format.		direction percentages from the traffic statistics.	
19	createFit_velocity	Traffic statistics in table format.	-	Distribution plot and normal fit for the traffic statistics: average velocity, number of axles, and maximal strain.	120
20	createFit_length	Traffic statistics in table format.	-	Distribution plot and normal fit for the traffic statistics: vehicles' length	126
21	plotEnergyDataLong_v2	SQL table name and fit distribution parameters	Structure with strain energy results.	Calculate the strain energy from all dynamic triggered events and plot the results.	674

Table 9. PCA related.

Pos.	Script name	Input argument	Output argument	Description	N° code lines
------	-------------	----------------	-----------------	-------------	---------------

22	collect_pca	Time-window size	Structure with PCA results.	Perform the PCA analysis for all dynamic strain history. The PCA is calculated for the moving time-window specified in the input argument.	466
23	collect_pca_short	Traffic statistics in table format and vehicle's length interval.	Structure with PCA results.	Performs the PCA analysis for all dynamic triggered events. The PCA is calculated for the events recorded in the traffic statistic table with vehicles within the length category.	121
24	collect_pca_average	Structure with PCA results.	Average PCA results.	Calculates the average PCA results for a vehicle length category	85
25	PCA_length	-	Multiple.	Perform multiple tasks: sort PCA results'	748

				<p>structure by length category, calculate the PCA for each length category, get the number of vehicle's crossings in each direction for each length category, plot PCA results for a length category, plot PCA results for all length categories in box plot format, calculate the PCA sensitivity about the length categories and plot in box plot format, and plot the sensitivity results in heatmap format</p>	
26	plot_eigenvalues	Structure with PCA results.	-	Plot selected PCA loadings for the inputted PCA structure.	181

27	plot_PCA_EXP	Structure with PCA results and length category index.	-	Plot PCA results and pareto with variance explanation for the inputted index.	60
28	plot_pca_groups	Structure with PCA results.	-	Plot PCA results for a length category.	163
29	plot_sensi_box	Structure with PCA sensitivity results.	-	Calculate the PCA sensitivity about the length categories and plot in box plot format.	295
30	plot_sensi_heat	Structure with PCA sensitivity results.	-	Calculate the PCA sensitivity about the length categories and plot the sensitivity results in heatmap format.	144
31	show_collect_pca	Structure with PCA results and FE simulation results.	Average PCA results for the inputted PCA structure.	Calculate the PCA results for the FE simulation and plot against the inputted length	304

				category's PCA results.	
32	plot_eigenvalues_hist	Structure with PCA results, travel direction, and sensor names.	PCA loadings and timestamp.	Plots the PCA results over time for the inputted sensors.	207

Table 10. FE model related.

Pos.	Script name	Input argument	Output argument	Description	N° code lines
33	annex_D	A pair of strain signals.	Standard variation results.	Perform the standard variation procedure between two signals accordingly to Annex D.8.2 Eurocode 0.	60
34	calc_PCA	Virtual SHM parameters and FE simulation results.	Virtual SHM strain signals.	Calculate the virtual SHM strain signals from the FE simulation results.	124
35	sens_eva	Type of normalization method.	Structure with PCA sensitivity results.	Calculate the PCA sensitivity from the FE simulation for the damage cases.	86

36	plot_final_damage	Final damages results.	-	Plot a heatmap with the final damages results from the FE model updating.	38
37	plot_PCA_NRMSE	Virtual SHM strain signals, reference PCA results.	-	Perform the PCA for the virtual SHM strain signals and plot against the reference PCA. For each PC, the NRMSE is calculated and plotted.	111
38	test_sobol	Structure with CA sensitivity results, reference PCA results, Monte Carlo simulation parameters.	PCA error improvement and final damages.	Run the Monte Carlo simulation to optimize the damage combination and intensity. The final damages correspond to the initial damaged model.	201
39	test_sobol2	Structure with CA sensitivity results, reference PCA results, Monte	PCA error improvement and final damages.	Run subsequent Monte Carlo simulations to refine the damage configuration	209

		Carlo simulation parameters.		and minimize the NRMSE.	
40	strain_points	Reference PCA results, virtual SHM results, and parameters.	Virtual SHM results and model accuracy.	Calculate the virtual SHM PCA results and analyze the NRMSE about the reference PCA results.	578
41	read_FEup	FE model updating iteration indexes.	NRMSE for each inputted iteration index.	Retrieve the NRMSE from the control spreadsheet file for the inputted iteration indexes. Plot the NRMSE with the respective gradient after each iteration.	138

Table 11. Rainflow analysis related.

Pos.	Script name	Input argument	Output argument	Description	N° code lines
42	load_count_data	-	-	Load the vehicle counting system results (located near the B27	209

				bridge) to a SQL table.	
43	read_count_data	Initial and final dates.	-	Plot the vehicle traffic counting results for the inputted date interval.	101
44	rainflow_hist	Rainflow analysis results' folder location.	-	Collect all rainflow results from the target folder and plot histograms.	299
45	rainflowCalc	Rainflow analysis results from a single file.	Histogram parameters.	Subroutine called by rainflow_hist to build the final histogram plots.	162

Table 12. Statistical strain mode and temperature related.

Pos.	Script name	Input argument	Output argument	Description	N° code lines
46	loop_Strain_Temp	-	Final strain mode vs. temperature matrix.	Collect the mean temperature and mean strain mode from the three-step check (real-time analysis) and plot them against each other.	43
47	read_Strain_Temp	Sensor information.	Strain mode	Subroutine called by loop_Strain_Temp	147

			and temperature results.	to access the SQL database and retrieve the strain mode and temperature results.	
--	--	--	--------------------------	--	--

8. List of publication

The publications originated from this research as pre-requisites for a cumulative doctoral dissertation are listed in Table 13.

Table 13. Cumulative doctoral dissertation: list of publications.

Num- ber	Publication	
	Title	
	Structural health monitoring of concrete structures using fibre-optic-based sensors: a review	
	Journal	Publisher
1	Magazine of Concrete Research	ICE, London, UK
	Status	DOI
	Published	https://doi.org/10.1680/jmacr.19.00185
	Title	
	A novel runtime algorithm for the real-time analysis and detection of unexpected changes in a real-size SHM network with quasi-distributed FBG sensors	
2	Journal	Publisher
	Sensors	MDPI, Basel, Switzerland
	Status	DOI
	Published	https://doi.org/10.3390/s21082871

Title	
Quantifying the actual damage level of a 60-year-old pre-stressed concrete bridge: a hybrid SHM approach	
Journal	Publisher
3 Structural Health Monitoring	SAGE, Thousand Oaks, CA, USA
Status	DOI
Under re-view	N.A.

Title	
Implemented scripts for the operation and data analysis of a real-size SHM based on long-gauge FBG sensors	
Journal	Publisher
4 Mendeley Data	Elsevier
Status	DOI
Published	http://dx.doi.org/10.17632/fmgdvwjgd5.1

References

- ABNT 2013, *Carga móvel rodoviária e de pedestres em pontes, viadutos, passarelas e outras estruturas*, ABNT, Rio de Janeiro, NBR 7188.
- Ahrens, MA & Sanio, D 2014, 'Wie lange noch?', *Forschung*, vol. 39, no. 3, pp. 26–31.
- Ahrens, MA, Strauss, A, Bergmeister, K, Mark, P & Stangenberg, F 2014, 'Lebensdauerorientierter Entwurf, Konstruktion, Nachrechnung' in *Beton-Kalender 2013. Lebensdauer und Instandsetzung-Behälter*, eds K Bergmeister, F Fingerloos & J-D Wörner, Wiley, Hoboken, pp. 17–222.
- Aicher, S, Leitschuh, N & Hezel, J 2015, *Abschlussbericht zum EFRE-Forschungsvorhaben „Stuttgarter Holzbrücke“: Projekt-Nr. 051203*.
- Alampalli, S & Lund, R 2006, 'Estimating Fatigue Life of Bridge Components Using Measured Strains', *Journal of Bridge Engineering*, vol. 11, no. 6, pp. 725–736.
- An, Y, Spencer, BF & Ou, J 2015, 'A Test Method for Damage Diagnosis of Suspension Bridge Suspender Cables', *Computer-Aided Civil and Infrastructure Engineering*, vol. 30, no. 10, pp. 771–784.
- Argebau 2019, *Konferenz der für Städtebau, Bau- und Wohnungswesen zuständigen Minister und Senatoren der Länder (Argebau), Bauministerkonferenz, 2002/ 27.09.2019*, Germany, Musterbauordnung (MBO), Fassung 2002.
- ASCOM/DNIT 2015, *Pontes e viadutos das rodovias federais estão em boas condições*, Brazil. Available from: <http://www.dnit.gov.br/noticias/pontes-e-viadutos-das-rodovias-federais-estao-em-boas-condicoes> [24 January 2016].
- Bao, X & Chen, L 2012, 'Recent progress in distributed fiber optic sensors', *Sensors (Basel, Switzerland)*, vol. 12, no. 7, pp. 8601–8639.
- Baqersad, J & Bharadwaj, K 2018, 'Strain expansion-reduction approach', *Mechanical Systems and Signal Processing*, vol. 101, pp. 156–167.
- Brownjohn, JMW 2007, 'Structural health monitoring of civil infrastructure', *Philosophical transactions. Series A, Mathematical, physical, and engineering sciences*, vol. 365, no. 1851, pp. 589–622.
- Catbas, FN, Gokce, HB & Gul, M 2012, 'Nonparametric analysis of structural health monitoring data for identification and localization of changes: Concept, lab, and real-life studies', *Structural Health Monitoring: An International Journal*, vol. 11, no. 5, pp. 613–626.
- Catbas, FN, Kijewski-Correa, TL & Aktan, AE 2013, *Structural identification of constructed systems. Approaches, methods, and technologies for effective practice of St-Id*, American Society of Civil Engineers, Reston Virginia.

- Cawley, P 2018, 'Structural health monitoring: Closing the gap between research and industrial deployment', *Structural Health Monitoring*, vol. 17, no. 5, pp. 1225–1244.
- Cegla, FB, Cawley, P, Allin, J & Davies, J 2011, 'High-temperature (500°C) wall thickness monitoring using dry-coupled ultrasonic waveguide transducers', *IEEE transactions on ultrasonics, ferroelectrics, and frequency control*, vol. 58, no. 1, pp. 156–167.
- Chen, S, Wu, G & Li, H 2018, 'Multi-scale finite element model updating of highway Multi-scale finite element model updating of highway bridge based on long-gauge strain response' in *Maintenance, Safety, Risk, Management and Life-Cycle Performance of Bridges. Proceedings of the Ninth International Conference on Bridge Maintenance, Safety and Management (LABMAS 2018), 9-13 July 2018, Melbourne, Australia*, eds N Powers, DM Frangopol, R Al-Mahaidi & C Caprani, Chapman and Hall/CRC, Milton, pp. 2820–2826.
- Cho, S, Giles, RK & Spencer, BF 2015, 'System identification of a historic swing truss bridge using a wireless sensor network employing orientation correction', *Structural Control and Health Monitoring*, vol. 22, no. 2, pp. 255–272.
- Chung, W, Kim, S, Kim, N-S & Lee, H-u 2008, 'Deflection estimation of a full scale prestressed concrete girder using long-gauge fiber optic sensors', *Construction and Building Materials*, vol. 22, no. 3, pp. 394–401.
- CNT 2015, *Pesquisa CNT de Ferrovias*, Brasília, Brazil.
- CNT, SEST & SENAT 2015, *Pesquisa CNT de rodovias 2015. Relatório gerencial*, Brasília, Brazil.
- Cremona, C & Santos, J 2018, 'Structural Health Monitoring as a Big-Data Problem', *Structural Engineering International*, vol. 28, no. 3, pp. 243–254.
- DIN 1999, *Ingenieurbauwerke im Zuge von Straßen und Wegen. Überwachung und Prüfung*, Beuth Verlag, Berlin, German, DIN 1076.
- Ehman, R 2006, *Spannungsrisikokorrosion von Spannstählen*, Karlsruhe, Germany.
- Europäisches Parlament, Rat der Europäischen Union 2011, *Verordnung (EU) Nr. 305/2011 des Europäischen Parlaments und des Rates vom 9. März 2011 zur Festlegung harmonisierter Bedingungen für die Vermarktung von Bauprodukten und zur Aufhebung der Richtlinie 89/106/EWG des Rates. Amtsblatt der Europäischen Union, L 88/5, 04.04.2011. Verordnung (EU) Nr. 305/2011.*
- Fackler, RM 2019, *Einsatz von faseroptischen Messsystemen mit FBGs an einer Spannbetonbrücke auf Basis von Laborversuchen*. Master's thesis.
- Farrar, CR & Worden, K 2007, 'An introduction to structural health monitoring', *Philosophical Transactions of The Royal Society*, pp. 303–315.

Fischer, O, Lechner, T, Wild, M, Müller, A & Kessner, K 2016, *Nachrechnung von Betonbrücken - systematische Datenauswertung nachgerechneter Bauwerke*, Fachverlag NW, Bremen.

Fouad, N, Saifelddeen, MA, Huang, H & Wu, Z 2018, 'Corrosion monitoring of flexural reinforced concrete members under service loads using distributed long-gauge carbon fiber sensors', *Structural Health Monitoring*, vol. 17, no. 2, pp. 379–394.

Frischmann, BM 2012, *Infrastructure. The social value of shared resources / Brett M. Frischmann*, Oxford University Press, New York.

Geobasis-de, B 2021, *Google Maps, city of Neckarsulm, Germany*, Google. Available from: <https://goo.gl/maps/NnYFGLB75pZYpJV16> [10 March 2021].

Giles, RK & Spencer Jr., BF 2015, 'Development of a long-term, multimetric structural health monitoring system for a historic steel truss swing bridge'.

Glisic, B 2011, 'Influence of the gauge length on the accuracy of long-gauge sensors employed in monitoring of prismatic beams', *Measurement Science and Technology*, vol. 22, no. 3, p. 35206.

Glisic, B & Inaudi, D 2012, 'Development of method for in-service crack detection based on distributed fiber optic sensors', *Structural Health Monitoring: An International Journal*, vol. 11, no. 2, pp. 161–171.

Glišić, B & Inaudi, D 2007, *Fibre optic methods for structural health monitoring*, John Wiley & Sons, Chichester West Sussex England, Hoboken NJ.

Goulet, JA & Smith, IFC 2013, 'Predicting the Usefulness of Monitoring for Identifying the Behavior of Structures', *Journal of Structural Engineering*, vol. 139, no. 10, pp. 1716–1727.

Goulet, J-A, Kripakaran, P & Smith, IFC 2010, 'Multimodel Structural Performance Monitoring', *Journal of Structural Engineering*, vol. 136, no. 10, pp. 1309–1318.

Hajdin, R 2018, 'Managing Existing Bridges – On the Brink of an Exciting Future' in *Maintenance, Safety, Risk, Management and Life-Cycle Performance of Bridges. Proceedings of the Ninth International Conference on Bridge Maintenance, Safety and Management (IABMAS 2018), 9-13 July 2018, Melbourne, Australia*, eds N Powers, DM Frangopol, R Al-Mahaidi & C Caprani, Chapman and Hall/CRC, Milton, pp. 70–87.

HBM FiberSensing S.A. 2021, *FS22 Industrial BraggMETER*. Available from: <https://www.hbm.com/de/4604/fs22-industrial-braggmeter-optischer-interrogator/> [18 February 2021].

Hong, W, Wu, Z, Yang, C, Wu, G & Zhang, Y 2015, 'Finite element model updating of flexural structures based on modal parameters extracted from dynamic distributed macro-strain responses', *Journal of Intelligent Material Systems and Structures*, vol. 26, no. 2, pp. 201–218.

- Hou, ST, Wu, G & Li, HL 2018, 'An Integrated Model-Based Bridge Management System' in *Maintenance, Safety, Risk, Management and Life-Cycle Performance of Bridges. Proceedings of the Ninth International Conference on Bridge Maintenance, Safety and Management (LABMAS 2018), 9-13 July 2018, Melbourne, Australia*, eds N Powers, DM Frangopol, R Al-Mahaidi & C Caprani, Chapman and Hall/CRC, Milton, pp. 198–204.
- Howell, DA & Shenton, HW 2006, 'System for In-Service Strain Monitoring of Ordinary Bridges', *Journal of Bridge Engineering*, vol. 11, no. 6, pp. 673–680.
- Huang, J, Zhou, Z, Zhang, D, Yao, X & Li, L 2016, 'Online monitoring of wire breaks in prestressed concrete cylinder pipe utilising fibre Bragg grating sensors', *Measurement*, vol. 79, pp. 112–118.
- Iodice, M, Striano, V, Cappuccino, G, Palumbo, A & Cocorullo, G 2005, 'Fiber Bragg grating sensors based system for strain measurements', *Proceedings of 2005 IEEE/LEOS Workshop on Fibres and Optical Passive Components*.
- Jaadi, Z 2019, *A Step-by-Step Explanation of Principal Component Analysis*. Available from: <https://builtin.com/data-science/step-step-explanation-principal-component-analysis>.
- Jang, S, Sim, S-H, Jo, H & Spencer, JBF 2011, 'Full-scale decentralized damage identification using wireless smart sensors', ed M Tomizuka, SPIE, 79814W.
- Kim, B, Min, C, Kim, H, Cho, S, Oh, J, Ha, S-H & Yi, J-H 2019, 'Structural Health Monitoring with Sensor Data and Cosine Similarity for Multi-Damages', *Sensors (Basel, Switzerland)*, vol. 19, no. 14.
- Krawtschuk, A, Strauß, A, Haider, K, Zimmermann, T & Bergmeister, K 2012, 'Ermittlung von Modellunsicherheiten bei Stahlbetonstrukturen', *Beton- und Stahlbetonbau*, vol. 107, no. 12, pp. 824–835.
- Krawtschuk, A, Wendner, R, Strauss, A & Bergmeister, K 2011, 'Sensitivity factor based model calibration and design evaluation', *fib Symposium, Prague*, pp. 487–490.
- Kudva, JN, Marantidis, C, Gentry, JD & Blazic, E 1993, 'Smart structures concepts for aircraft structural health monitoring', eds NW Hagood & GJ Knowles, SPIE, pp. 964–971.
- Laory, I, Trinh, TN, Posenato, D & Smith, IFC 2013, 'Combined Model-Free Data-Interpretation Methodologies for Damage Detection during Continuous Monitoring of Structures', *Journal of Computing in Civil Engineering*, vol. 27, no. 6, pp. 657–666.
- Laory, I, Trinh, TN & Smith, IFC 2011, 'Evaluating two model-free data interpretation methods for measurements that are influenced by temperature', *Advanced Engineering Informatics*, vol. 25, no. 3, pp. 495–506.
- Lehmann, FA 2020, 'Non-destructive testing and monitoring as elements of building inspection', *Otto-Graf-Journal*, vol. 19, pp. 119–130.

- Lehmann, FA, Sakiyama, FIH & Fackler, RM 2019, 'Fibre optic measurement systems for building monitoring', *Otto-Graf-Journal*, vol. 18, pp. 183–196.
- Li, H-N, Li, D-S & Song, G-B 2004, 'Recent applications of fiber optic sensors to health monitoring in civil engineering', *Engineering Structures*, vol. 26, no. 11, pp. 1647–1657.
- Li, J, Mechitov, KA, Kim, RE & Spencer, BF 2016, 'Efficient time synchronization for structural health monitoring using wireless smart sensor networks', *Structural Control and Health Monitoring*, vol. 23, no. 3, pp. 470–486.
- Lopez-Higuera, JM, Rodriguez Cobo, L, Quintela Incera, A & Cobo, A 2011, 'Fiber Optic Sensors in Structural Health Monitoring', *Journal of Lightwave Technology*, vol. 29, no. 4, pp. 587–608.
- Lünser, H 1999, *Ökobilanzen im Brückenbau. Eine umweltbezogene, ganzheitliche Bewertung*, Birkhäuser, Basel.
- Lydon, D, Lydon, M, Kromanis, R, Dong, C-Z, Catbas, N & Taylor, S 2021, 'Bridge Damage Detection Approach Using a Roving Camera Technique', *Sensors (Basel, Switzerland)*, vol. 21, no. 4.
- Lynch, JP 2007, 'An overview of wireless structural health monitoring for civil structures', *Philosophical Transactions of The Royal Society*, pp. 345–372.
- Mahadevan, S, Adams, D & Kosson, D 2014, 'Challenges in Concrete Structures Health Monitoring' in *Annual Conference of the Prognostics and Health Management Society 2014*, eds MJ Daigle & A Bregon, Fort Worth, TX, USA, pp. 561–567.
- MATLAB*. version 9.9.0 (R2020b) 2020, The MathWorks, Inc., Natick, Massachusetts.
- Mendes, PC 2009, *Contribuições para um modelo de gestão de pontes de concreto aplicado à rede de rodovias brasileiras*. Ph.D., São Paulo.
- Metzger, AT & Huckelbridge, AA 2009, *Temporal Nature of Fatigue Damage in Highway Bridges*, National Fire Protection Assoc, Quincy MA.
- MySQL Workbench 8.0* 2020, Oracle Corporation, Redwood City, California.
- Okasha, NM, Frangopol, DM & Orcesi, AD 2012, 'Automated finite element updating using strain data for the lifetime reliability assessment of bridges', *Reliability Engineering & System Safety*, vol. 99, pp. 139–150.
- Phares, B, Lu, P, Wipf, T, Greimann, L & Seo, J 2013, 'Field Validation of a Statistical-Based Bridge Damage-Detection Algorithm', *Journal of Bridge Engineering*, vol. 18, no. 11, pp. 1227–1238.
- Piyasena, R 2003, *Crack Spacing, Crack Width and Tension Stiffening Effect in Reinforced Concrete Beams and One-Way Slabs*. PhD, Griffith University, Queensland, Australia.

Posenato, D, Kripakaran, P, Inaudi, D & Smith, IFC 2010, 'Methodologies for model-free data interpretation of civil engineering structures', *Computers & Structures*, vol. 88, 7-8, pp. 467–482.

Posenato, D, Lanata, F, Inaudi, D & Smith, IFC 2008, 'Model-free data interpretation for continuous monitoring of complex structures', *Advanced Engineering Informatics*, vol. 22, no. 1, pp. 135–144.

Rommerskirchen, S, Rothengatter, W, Greinus, A, Leyboldt, P, Liedtke, G & Scholz, A 2007, *Aktualisierung der Wegekostenrechnung für die Bundesfernstraßen in Deutschland. Endbericht A15/315.4/7-03.2*, Basel/Karlsruhe.

Sakiyama, FIH 2021, *Implemented scripts for the operation and data analysis of a real-size SHM based on long-gauge FBG sensors*.

Sakiyama, FIH, Lehmann, F & Garrecht, H 2021a, 'A Novel Runtime Algorithm for the Real-Time Analysis and Detection of Unexpected Changes in a Real-Size SHM Network with a Quasi-Distributed FBG Sensors', *Sensors*, vol. 21, no. 8, p. 2871.

Sakiyama, FIH, Lehmann, F & Garrecht, H 2021b, 'Structural health monitoring of concrete structures using fibre-optic-based sensors: a review', *Magazine of Concrete Research*, vol. 73, no. 4, pp. 174–194.

Sakiyama, FIH, Veríssimo, GS, Lehmann, F & Garrecht, H in press, 'An integrated methodology for data interpretation and model updating in a real-size SHM network based on long-gauge FBG strain sensors', *Structural Health Monitoring*.

Sanio, D, Ahrens, MA, Mark, P & Rode, S 2014, 'Untersuchung einer 50 Jahre alten Spannbetonbrücke zur Genauigkeitssteigerung von Lebensdauerprognosen', *Beton- und Stahlbetonbau*, vol. 109, no. 2, pp. 128–137.

Santos, JP, Crémona, C, Calado, L, Silveira, P & Orcesi, AD 2016, 'On-line unsupervised detection of early damage', *Structural Control and Health Monitoring*, vol. 23, no. 7, pp. 1047–1069.

Santos, JP, Orcesi, AD, Crémona, C & Silveira, P 2015, 'Baseline-free real-time assessment of structural changes', *Structure and Infrastructure Engineering*, vol. 11, no. 2, pp. 145–161.

Sehgal, S & Kumar, H 2016, 'Structural Dynamic Model Updating Techniques: A State of the Art Review', *Archives of Computational Methods in Engineering*, vol. 23, no. 3, pp. 515–533.

Song, J-H, Lee, E-T & Eun, H-C 2021, 'Optimal sensor placement through expansion of static strain measurements to static displacements', *International Journal of Distributed Sensor Networks*, vol. 17, no. 1, 155014772199171.

Spencer, BF, Jo, H, Mechtov, KA, Li, J, Sim, S-H, Kim, RE, Cho, S, Linderman, LE, Moïnzadeh, P, Giles, RK & Agha, G 2016, 'Recent advances in wireless smart sensors

for multi-scale monitoring and control of civil infrastructure', *Journal of Civil Structural Health Monitoring*, vol. 6, no. 1, pp. 17–41.

Spencer, BF, Ruiz-Sandoval, ME & Kurata, N 2004, 'Smart sensing technology: opportunities and challenges', *Structural Control and Health Monitoring*, vol. 11, no. 4, pp. 349–368.

Strauss, A, Wendner, R, Bergmeister, K, Reiterer, M & Horvatits, J 2011, 'Modellkorrekturfaktoren als "Performance Indikatoren" für die Langzeitbewertung der integralen Marktwasserbrücke S33.24', *Beton- und Stahlbetonbau*, vol. 106, no. 4, pp. 231–240.

Strauss, A, Wendner, R, Frangopol, DM & Bergmeister, K 2012, 'Influence line model correction approach for the assessment of engineering structures using novel monitoring techniques', *Smart Structures and Systems*, vol. 9, no. 1, pp. 1–20.

Sun, H & Büyüköztürk, O 2015, 'Optimal sensor placement in structural health monitoring using discrete optimization', *Smart Materials and Structures*, vol. 24, no. 12, p. 125034.

Sylex s.r.o 2021, *SC-01 Strain cable sensor*. Available from: <https://www.sylex.sk/product/sc-01-strain-cable-sensor/> [18 February 2021].

Udd, E & Inaudi, D (eds.) 2005, *Demodulating interferometric and FBG sensors in the spectral domain*, SPIE.

Udd, E & Spillman, WB 2011, *Fiber optic sensors. An introduction for engineers and scientists*, John Wiley & Sons, Hoboken N.J.

Waibel, P, Schneider, O, Keller, HB, Müller, J & Keller, S 2018, 'A strain sensor based monitoring and damage detection system for a two-span beam bridge' in *Maintenance, Safety, Risk, Management and Life-Cycle Performance of Bridges. Proceedings of the Ninth International Conference on Bridge Maintenance, Safety and Management (LABMAS 2018), 9-13 July 2018, Melbourne, Australia*, eds N Powers, DM Frangopol, R Al-Mahaidi & C Caprani, Chapman and Hall/CRC, Milton, pp. 1627–1634.

Wang, H, Jiang, L & Xiang, P 2018, 'Priority design parameters of industrialized optical fiber sensors in civil engineering', *Optics & Laser Technology*, vol. 100, pp. 119–128.

Worden, K & Dulieu-Barton, JM 2004, 'An Overview of Intelligent Fault Detection in Systems and Structures', *Structural Health Monitoring: An International Journal*, vol. 3, no. 1, pp. 85–98.

Wu, B, Wu, G, Yang, C & He, Y 2016, 'Damage identification and bearing capacity evaluation of bridges based on distributed long-gauge strain envelope line under moving vehicle loads', *Journal of Intelligent Material Systems and Structures*, vol. 27, no. 17, pp. 2344–2358.

- Wüstholtz, T 2016, 'Instandsetzung oder Neubau von Massivbrücken? Erfahrungen und davon abgeleitete Ansätze'. *Instandhaltung von Wasserbauwerken. Kolloquium am 25. und 26. Oktober 2016*, ed Bundesanstalt für Wasserbau (Hg.), BAW, Karlsruhe, Germany, pp. 23–41.
- Xiao, F, Hulsey, JL, Chen, GS & Xiang, Y 2017, 'Optimal static strain sensor placement for truss bridges', *International Journal of Distributed Sensor Networks*, vol. 13, no. 5, 155014771770792.
- Xu, Z-D, Liu, M, Wu, Z & Zeng, X 2011, 'Energy Damage Detection Strategy Based on Strain Responses for Long-Span Bridge Structures', *Journal of Bridge Engineering*, vol. 16, no. 5, pp. 644–652.
- Ye, XW, Su, YH & Han, JP 2014, 'Structural health monitoring of civil infrastructure using optical fiber sensing technology: a comprehensive review', *TheScientificWorldJournal*, vol. 2014, p. 652329.
- Ye, X-W, Su, Y-H & Xi, P-S 2018, 'Statistical Analysis of Stress Signals from Bridge Monitoring by FBG System', *Sensors (Basel, Switzerland)*, vol. 18, no. 2.
- Zhang, J, Guo, SL, Wu, ZS & Zhang, QQ 2015a, 'Structural identification and damage detection through long-gauge strain measurements', *Engineering Structures*, vol. 99, pp. 173–183.
- Zhang, J, Xia, Q, Cheng, Y & Wu, Z 2015b, 'Strain flexibility identification of bridges from long-gauge strain measurements', *Mechanical Systems and Signal Processing*, 62-63, pp. 272–283.
- Zhou, YE 2006, 'Assessment of Bridge Remaining Fatigue Life through Field Strain Measurement', *Journal of Bridge Engineering*, vol. 11, no. 6, pp. 737–744.
- Zhu, Y, Ni, Y-Q, Jin, H, Inaudi, D & Laory, I 2019, 'A temperature-driven MPCA method for structural anomaly detection', *Engineering Structures*, vol. 190, pp. 447–458.

Curriculum vitae

PERSONAL DATA

Felipe Isamu Harger Sakiyama

felipe.sakiyama@ufvjm.edu.br isamuu@gmail.com

Born on 23rd December 1988

EDUCATION

2012-2015 M.Sc. in Civil Engineering from Universidade Federal de Viçosa (UFV), Brazil

2007-2012 Bachelor's degree in civil engineering from Universidade Federal de Viçosa (UFV), Brazil

2004-2006 Secondary School Colégio de Aplicação da Universidade Federal de Viçosa (COLUNI), Brazil

1997-2003 Primary School Colégio Normal Nossa Senhora do Carmo in Viçosa, Brazil

1996 Primary School Colégio Nossa Senhora da Auxiliadora (CENSA) in Campos dos Goytacazes, Brazil

PROFESSIONAL EXPERIENCE

2013 – present UNIVERSIDADE FEDERAL DOS VALES DO JEQUITINHONHA E MUCURI – UFVJM

Assistant Professor

Institute of Science, Engineering and Technology

SCHOLARSHIP

2017-2021 CAPES Scholarship Holder